Contents lists available at ScienceDirect

Arabian Journal of Chemistry

journal homepage: www.ksu.edu.sa

An extended strategy of "Recursive Tree" for characterization of drug metabolites *in vivo* and *in vitro* and actional mechanism study based on network Pharmacology: Formononetin as a study case

Yanan Li [a,c], Shaoping Wang [b], Hong Wang [a,d], Long Dai [b,c], Jiayu Zhang [a,*]

[a] School of Traditional Chinese Medicine, Binzhou Medical University, Yantai 264003, China
[b] School of Pharmacy, Binzhou Medical University, Yantai 264003, China
[c] School of Pharmacy, Shandong University of Traditional Chinese Medicine, Jinan 250355, China
[d] College of Life Sciences, Shandong Agricultural University, Taian 271018, China

ARTICLE INFO

Keywords:
Recursive tree analytical strategy
Metabolism
Network pharmacology
Formononetin
NAFLD
UHPLC-Q-Exactive Orbitrap MS

ABSTRACT

The screening and identification of drug metabolites in biological matrices is challenging, and ultra-high performance liquid chromatography-Q-Exactive Orbitrap mass spectrometry (UHPLC-Q-Exactive Orbitrap MS) has become a powerful technological tool for drug metabolites analysis due to its high sensitivity. However, the spectral information contained in existing chemical standards and databases is very limited, and the UHPLC-Q-Exactive Orbitrap MS technique alone cannot satisfy the identification of complex and diverse metabolites. Therefore, there is an urgent need for a new strategy to achieve comprehensive drug metabolic profile. Based on this, we have innovatively constructed a "recursive tree" analysis strategy and bridged it with network pharmacology for elucidating the pharmacological mechanisms of drugs. In this paper, we investigated the overall metabolic profile of formononetin as an example and utilized the primary branching metabolites of formononetin as effective ingredients for the study of the anti-NAFLD mechanism. The results showed that a total of 131 metabolites (prototype drug included) were detected and identified. Among them, 106 metabolites were found in rats and 31 metabolites were found in liver microsomes. Glucose conjugation, demethylation, sulfation, glucuronidation, and their complex reactions were the major processes of formononetin biotransformation. Network pharmacology results screened 104 potential targets and 20 major signaling pathways. Their mechanisms may be additive and/or synergistic effects. In addition, the therapeutic effects of formononetin against NAFLD were investigated based on palmitic acid / oleic acid-induced HepG2 cells. In summary, the recursive tree analysis strategy provides a convenient method for the identification of metabolites, and its seamless integration with network pharmacology lays the foundation for studying the pharmacological activities of natural products.

1. Introduction

Drug metabolism is the process by which exogenous compounds undergo chemical structural changes catalyzed by various enzymes in the body, also known as biotransformation (Almazroo et al., 2017). It can transform exogenous compounds into active metabolites or toxic metabolites, generally known as the duality of biotransformation (Klotz et al., 2009). Metabolites may be the "effective form" of drugs due to their high blood concentration (Knights et al., 2016). Therefore, metabolic profiles are essential for elucidating the actional mechanism of

Abbreviations: NAFLD, anti-nonalcoholic fatty liver disease; DPIs, diagnostic product ions; PRM, parallel reaction monitoring; NLFs, neutral loss fragments; SD, Sprague Dawley; $MgCl_2$, Magnesium chloride; UDPGA, uridine 5′-diphosphoglucuronic acid trisodium salt; NADPH, β-nicotinamine adenine dinucleotide phosphate; PA/OA, palmitic acid / oleic acid; BCA, bicinchoninic acid; TG, total triglycerides; TC, total cholesterol; ALT, alanine transaminase; AST, aspartate transaminase; SOD, superoxide dismutase; GSH, glutathione peroxidase; CCK-8, Cell Counting Kit-8; FA, formic acid; RDB, ring double bond; NF-κB, nuclear factor kappa-B; AKT1, AKT serine/threonine kinase 1; FoxO, forkhead box O3; ALB, albumin; MAPK, mitogen-activated protein kinase; IL-17, interleukin 17; STAT3, signal transducer and activator of transcription 3; PI3K, phosphatidylinositol-3-kinases; EGFR, epidermal growth factor receptor; Akt, protein-serine-threonine kinase; mTOR, mammalian target of rapamycin.

* Corresponding author at: School of Traditional Chinese Medicine, Binzhou Medical University, Yantai, 264003, Shandong, China.
E-mail address: zhangjiayu0615@163.com (J. Zhang).

https://doi.org/10.1016/j.arabjc.2024.105761
Received 4 February 2024; Accepted 24 March 2024
Available online 26 March 2024

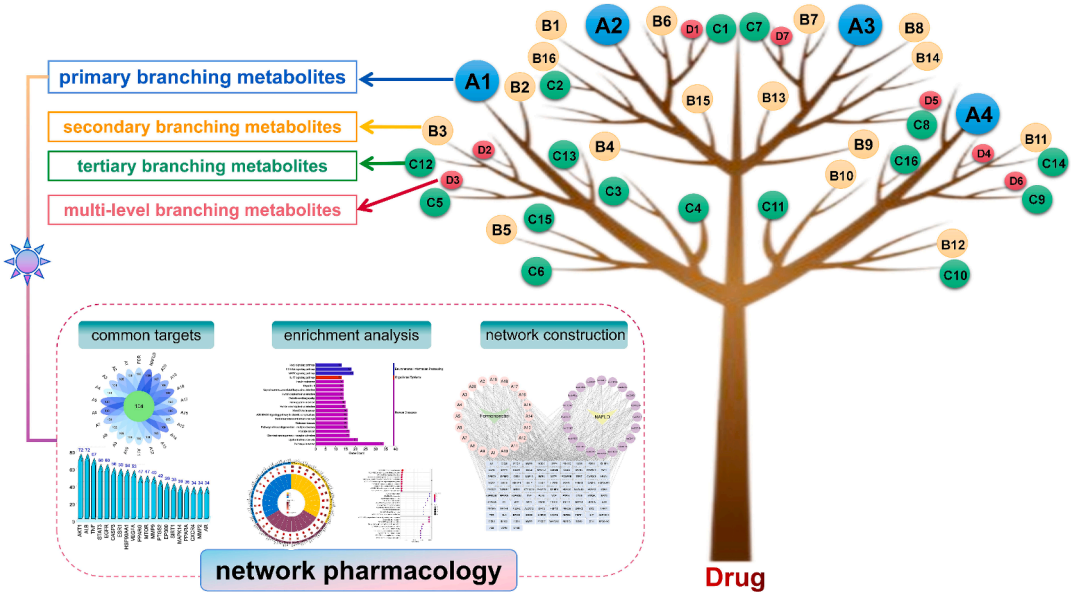

Fig. 1. The summary diagram of recursive tree analysis strategy.

drugs. However, hundreds of metabolites make it difficult to conduct actional mechanism studies based on all metabolites. Thus, rational selection of metabolites for mechanism studies is particularly important.

In recent years, the research on drug metabolites has made deeper development. Ultra-high performance liquid chromatography-Q-Exactive Orbitrap mass spectrometry (UHPLC-Q-Exactive Orbitrap MS) has been widely used for metabolite research with its high resolution, high sensitivity, and high accuracy (Wang et al., 2019). Moreover, the use of techniques such as neutral loss fragments (NLFs), diagnostic product ions (DPIs), and parallel reaction monitoring (PRM) has enabled high-quality mass spectrometry data acquisition, but data mining strategies for metabolites remain to be further developed (Knights et al., 2016; Kaur et al., 2020). Based on this, we first propose the "recursive tree" analysis strategy, which draws on the ideas of induction and deduction, starting from the prototype drugs and progressing step by step. In addition, network pharmacology is used to reveal the interrelationships between effective ingredients and actional targets through multidisciplinary cross-applications and integration of holistic biological networks based on bioinformatics methods (Yin et al., 2019; Das et al., 2018). Primary branching metabolites have higher blood concentrations and biological activity compared to prototypical compounds, making them most likely to be the main material basis for the treatment of disease (Cui et al., 2022; Cai et al., 2020). Therefore, the combination of these metabolites with network pharmacology can elucidate the synergistic mechanism of action between metabolites and improve the accuracy of modern pharmacological studies and the mechanism of exploration of drugs.

Formononetin (7-hydroxy-4′-methoxy isoflavone) widely distributes in Leguminosae plants, such as *Glycyrrhiza uralensis* Fisch (Zhao et al., 2021), *Astragalus membranaceus* (Liu et al., 2021), *Pueraria lobata* (Li et al., 2016), *Trifolium pretense* (Muñoz et al., 2022), and *Santalum album* (Machado et al., 2021). Over the past decade, formononetin has been intensively studied and many biological activities have been reported, including anti-inflammatory (Yu et al., 2022), antioxidant (Li et al., 2022), antitumor (Ma et al., 2022), vasodilatory (Oza et al., 2019), neuroprotective effects (Aly et al., 2021), and so on. It is worth mentioning that the potential anti-NAFLD effects of formononetin have been reported, but the specific mechanism and the material basis are still unclear. Several studies have investigated the pharmacokinetics of formononetin after oral administration in humans, rats, or mice (Rao et al., 2019; Guo et al., 2015; Kim et al., 2022). However, the metabolic profile remains incomplete. Due to the potential therapeutic role of formononetin in NAFLD (Scorletti et al., 2022), a deeper understanding of its metabolic fate is essential. As there is no systematic analytical strategies or techniques to mine and characterize formononetin metabolites, the screening of formononetin metabolites from complex matrix systems remains a difficult task in metabolic studies.

In this study, the formononetin was used as a case study. For the first time, the recursive tree analysis strategy was proposed and combined with multiple data processing tools to quickly screen and identify the metabolites of formononetin *in vivo* and *in vitro*. What's more, the primary branching metabolites of formononetin were bridged with network pharmacology, and the actional mechanism of formononetin against NAFLD was initially elucidated.

2. Materials and methods

2.1. Chemicals and reagents

Formononetin reference (Batch number: MUST-21033005, purity ≥ 99.03 %) and Ononin reference (Batch number: MUST-21080311, purity ≥ 98.48 %) were provided by Chengdu Must Biotechnology Co., Ltd. (Sichuan, China). HepG2 cells was obtained from Binzhou medical university (Yantai, China). Kits measuring the levels of bicinchoninic acid (BCA), total cholesterol (TC), total triglycerides (TG), alanine transaminase (ALT), aspartate transaminase (AST), superoxide dismutase (SOD), and glutathione peroxidase (GSH) were purchased from Jiancheng Institute of Biotechnology (Nanjing, China). Palmitic acid / oleic acid (PA/OA) were obtained Xi'an Kunchuang Technology Development Co., Ltd. (Xian, China). Oil Red O and Cell Counting Kit-8 (CCK-8) were purchased from Beyotime Biotechnology (Shanghai, China).

HPLC grade methanol, acetonitrile, and formic acid (FA) were purchased from Thermo Fisher Scientific (Fair Lawn, NJ, USA), and pure water for analysis was purchased from Watson Group Co., Ltd. (Jinan, China). All the other chemicals of analytical grade were available at the workstation, Shandong Academy of Chinese Medicine (Jinan, China). Grace Pure^{TM} SPE C18-Low solid phase extraction cartridges (200 mg·3 mL^{-1}, 59 μm, 70 Å) were purchased from Grace Davison Discovery Science (Deerfield, IL, USA). Male Sprague Dawley (SD) rat liver

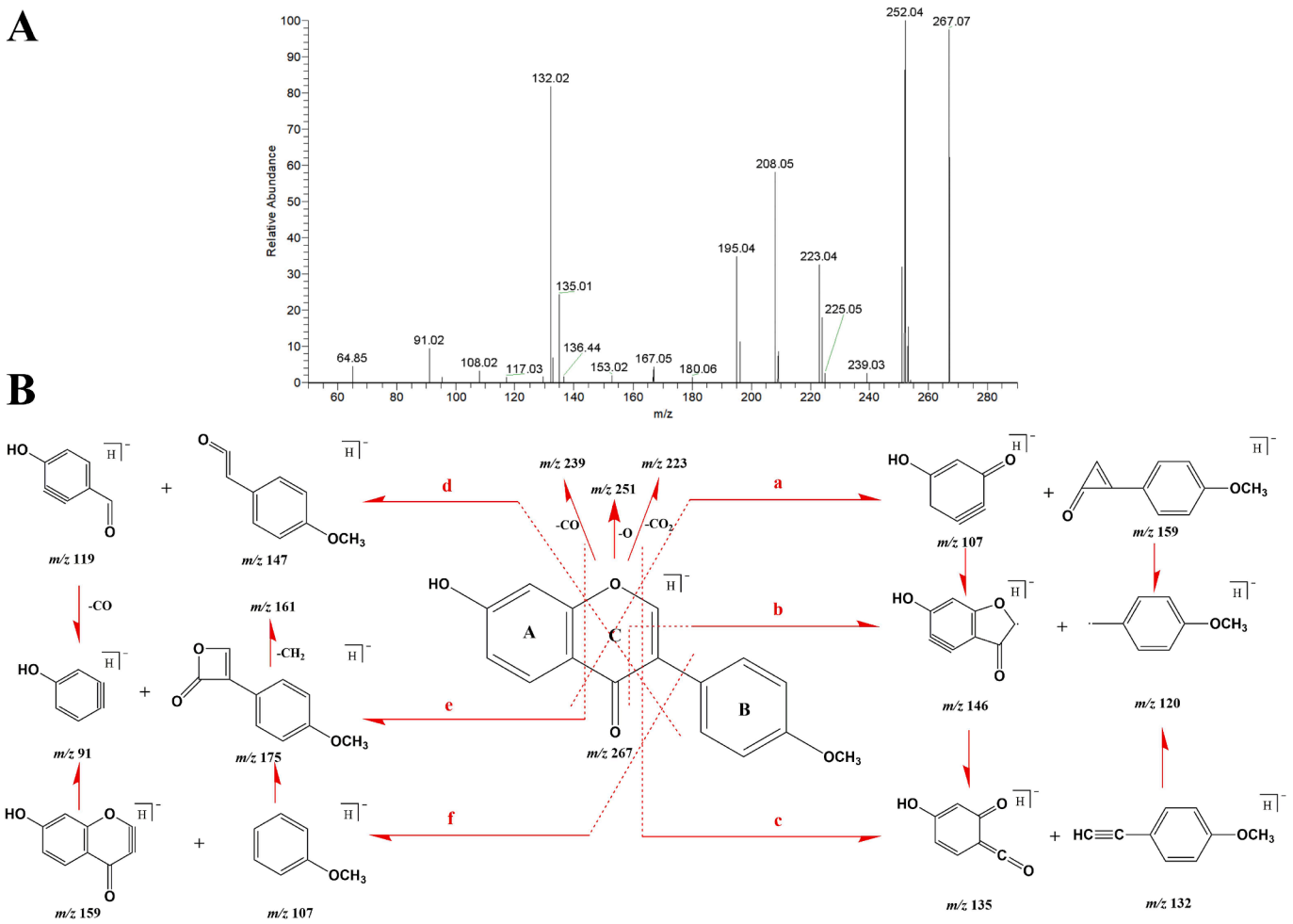

Fig. 2. ESI-MS spectrum (A) and typical cleavage pathways (B) of formononetin in negative ion mode.

microsomes (1 mL, Batch number: 20210305), Magnesium chloride ($MgCl_2$), β-nicotinamine adenine dinucleotide phosphate (NADPH), and uridine 5′-diphosphoglucuronic acid trisodium salt (UDPGA) were all purchased from NEWGAINBIO Co., Ltd. (Wuxi, China).

2.2. In vivo animal experiment

2.2.1. Animals and drug administration

Eight male SD rats (200 ± 10 g) were acquired by Jinan Pengyue Experimental Animal Technology Co., Ltd. (Jinan, China). They were free to drink and eat at humidity (70 ± 5 %) and constant temperature (25 ± 2 °C) for 7 days. The rats were randomly divided into two groups including Formononetin Group (n = 6) and Control Group (n = 6) for test plasma, urine, faeces, and liver, respectively. They were fasted for 12 h with free access to water before the experiment. Formononetin was dissolved in 0.9 % saline solution. The rats in the formononetin group and the control group were orally administered with formononetin solution (150 $mg{\cdot}kg^{-1}$, 10 $mL{\cdot}kg^{-1}$) and 0.9 % saline solution, respectively. Pentobarbital sodium was used for anesthesia. The animal facilities and protocols were complied with the Guide for the Care and Use of Laboratory Animals (USA National Research Council, 1996). The animal experiment was approved by the Animal Care and Use Committee at Binzhou Medical University (2021–085).

2.2.2. Sample collection and pretreatment

Plasma samples were prepared by collecting blood samples from the infraorbital venous plexus within 24 h and centrifuging at 3,500 rpm for 10 min. Urine and faeces samples were collected from the metabolic cage within 24 h. Furthermore, liver samples were collected and quenched in liquid nitrogen from dissected rats. Finally, the collected homogeneous samples were mixed. (Li et al., 2022).

The main method of sample pretreatment is the SPE cartridges purification method. To obtain more metabolites, methanol precipitation, and acetonitrile precipitation methods were added to the pretreatment of plasma samples. Specific research methods were described in the team's previous research. (Li et al., 2022; Dong et al., 2021; Wang et al., 2022; Jing et al., 2022).

2.3. In vitro liver microsomes incubation

Firstly, incubation mixtures were prepared in PBS buffer and divided into Drug Group and the Control Group. The buffer for the Drug Group contained rat liver microsomes (1 $mg{\cdot}mL^{-1}$), formononetin (0.1 $mg{\cdot}mL^{-1}$), and $MgCl_2$ (3 mM, final concentration). The buffer for the Control Group did not contain formononetin. 900 μL of the above incubation mixture, 100 μL of NADPH (25 $mg{\cdot}mL^{-1}$) and 100 μL of UDPGA (25 $mg{\cdot}mL^{-1}$) were added to each of the 6-well plates to start the reaction. The reaction was incubated at 37 °C for 5, 10, 15, 30, 45, 60, 120, 240, and 480 min, and then 100 μL of incubation solution was removed and the reaction was terminated by adding 200 μL of cold acetonitrile. Finally, the supernatant was purified by acetonitrile precipitation.

2.4. Instruments and analytical conditions

UHPLC analysis was conducted on the Dionex Ultimate 3000 UHPLC

Table 1
Summary of formononetin metabolites *in vivo* and *in vitro*.

ID	Ion Mode	t_R/ min	Formula [M−H]⁻/ [M+H]⁺	Theoretical Mass (*m/z*)	Experimental Mass (*m/z*)	RDB	Error (ppm)	MS/MS Fragment Ions	PS	PM	PA	U	F	L	LM
formononetin	N	9.62	$C_{16}H_{11}O_4$	267.06519	267.06631	11.5	0.104	252(100),267(89),221(2),206(1),134(2),121(5),194(2),102(1),92(2),77(1)	+	+	+	+	+	+	+
	P	9.63	$C_{16}H_{13}O_4$	269.08083	269.08026	12.5	0.156	269(100),253(46),136(24),223(5),225(8),211(5),161(11)	+	+	+	+	+	−	+
A1	P	6.92	$C_{22}H_{23}O_9$	431.13409	431.13365	10.5	1.000	269(100),431(2),253(1),136(1),161(1)	−	−	−	−	−	−	+
A2	N	7.09	$C_{15}H_9O_4$	253.04953	253.05043	11.5	−0.799	253(100),225(18),209(5),237(2),221(2)	+	−	+	−	−	−	−
	P	7.09	$C_{15}H_{11}O_4$	255.06518	255.06427	10.5	−0.915	255(100),199(6),137(4),227(3),91(1)	+	+	+	+	+	−	−
A3	N	8.22	$C_{16}H_{11}O_7S$	347.02199	347.02319	11.5	0.269	267(100),347(33),252(31),62(2),223(2)	+	+	+	−	−	−	−
	P	8.23	$C_{16}H_{13}O_7S$	349.03764	349.03650	10.5	−1.150	269(100),349(31),254(4),213(3),97(3)	+	+	−	−	−	−	−
A4	N	6.97	$C_{22}H_{19}O_{10}$	443.09727	443.09888	13.5	0.045	267(100),107(73),252(53),209(35),443(32)	+	−	+	+	−	−	−
	P	6.97	$C_{22}H_{21}O_{10}$	445.11292	445.11172	12.5	−1.873	269(100),445(10),254(2),213(1),237(1)	+	+	−	+	−	−	−
A5	P	4.81	$C_{16}H_{13}O_5$	285.07575	285.07498	10.5	−0.770	285(100),137(63),270(18),149(2),63(1)	+	−	−	−	−	−	−
A6	N	6.12	$C_{16}H_{11}O_5$	283.06009	283.06119	11.5	−0.024	135(100),283(58),240(4),211(2),147(1)	−	−	−	−	−	−	+
A7	N	6.81	$C_{16}H_{11}O_5$	283.06009	283.06125	11.5	0.188	283(100),135(63),163(18),120(2),147(1)	−	−	−	−	−	−	+
A8	N	7.30	$C_{16}H_{11}O_5$	283.06009	283.06116	11.5	−0.130	268(100),283(72),135(22),147(17),61(6)	−	−	−	+	−	−	−
A9	N	7.85	$C_{16}H_{11}O_5$	283.06009	283.06097	11.5	−0.801	283(100),268(61),135(20),175(2),147(1)	−	−	−	−	−	−	+
A10	N	8.76	$C_{16}H_{11}O_5$	283.06009	283.06100	11.5	−0.695	283(100),268(77),224(5),132(3),152(0.6)	−	−	−	−	−	−	+
A11	N	9.52	$C_{16}H_{11}O_5$	283.06009	283.06116	11.5	−0.130	283(100),268(74),224(11),152(9),132(6)	−	−	−	−	−	−	+
A12	P	10.66	$C_{16}H_{13}O_5$	285.07575	285.07477	10.5	−0.980	285(100),270(54),134(11),154(9),63(6)	−	−	−	−	−	−	+
A13	N	10.84	$C_{17}H_{13}O_4$	281.08083	281.08194	11.5	0.028	253(100),281(79),223(3),134(2),232(1)	−	−	−	−	−	−	+
	P	10.87	$C_{17}H_{15}O_4$	283.09648	283.09564	10.5	−2.986	283(100),255(26),93(9),163(7),206(6)	−	−	−	+	−	−	−
A14	N	7.21	$C_{16}H_{13}O_4$	269.08083	269.08200	10.5	0.252	269(100),225(7),253(5),135(4),209(3)	−	−	−	+	−	−	−

system (Thermo Fisher Scientific, MA, USA). Separation was performed on a Waters ACQUITY UPLC BEH C18 column (2.1 × 100 mm, 1.7 μm). The column temperature was kept at 30℃, the flow rate was 0.3 mL·min^{-1}. The mobile phase was composed of water containing 0.1 % formic acid (A) and acetonitrile (B). The elution gradient condition was as follows: 0–5 min, 5 %-30 % B; 5–10 min, 30 %-50 % B; 10–27 min, 50 %-90 % B; 27–27.1 min, 90 %-5% B; 27.1–30 min, 5 % B.

HRMS and MS/MS spectra were obtained using Q-Exactive Focus Orbitrap MS (Thermo Fisher, Waltham, MA, USA) equipped with HESI. The ion source parameters were set as follows: Scan range, *m/z* 80–1,200; Aux gas flow rate, 10 arbitrary units; Aux gas heater temperature, 320 °C; Sheath gas flow rate, 45 arbitrary units; Capillary temperature, 320 °C; Spray voltage, 3.8/3.5 kV (+/-); Scan modes, full MS resolution, 70,000; dd-MS^2 resolution, 17,500; Collision energy, 15 %, 30 %, 45 %.

2.5. Data processing and peak selections

In order to obtain accurate metabolites of formononetin, the parameters of the Thermo Xcalibur 2.1 workstation were set within a reasonable range. The compositional structural formulae were set to C [0–30], N[0–5], O[0–15], H[0–60], S[0–1]. The mass error range was set to within ± 5 ppm. The ring double bond (RDB) equivalent was set to [0–15].

2.6. Cells and treatments

Logarithmic growth phase HepG2 cells were inoculated into 96-well plates at a density of 5 × 10^3 per well for cell viability. Subsequently, HepG2 cells were seeded into 6-well plates at a density of 2 × 10^5 per well. The cells were stimulated with PA (187.5 μM) / OA (375 μM) and formononetin (5, 10, and 50 μg·mL^{-1}) for 24 h. After fixation with 4 % paraformaldehyde, Oil Red O staining was added for 20 min, and the images were captured using an Echo Laboratories RevolveFL imaging system (San Diego, USA). Finally, HepG2 cells were collected by inoculating 6-well plates in the same way to determine protein content. The levels of TC, TG, AST, ALT, SOD, and GSH were also determined according to the kit instructions.

2.7. Network pharmacology

2.7.1. Targets prediction and screening common targets

Formononetin and its primary branch metabolites were subjected to a SMILE search in the PubChem database and relevant targets were

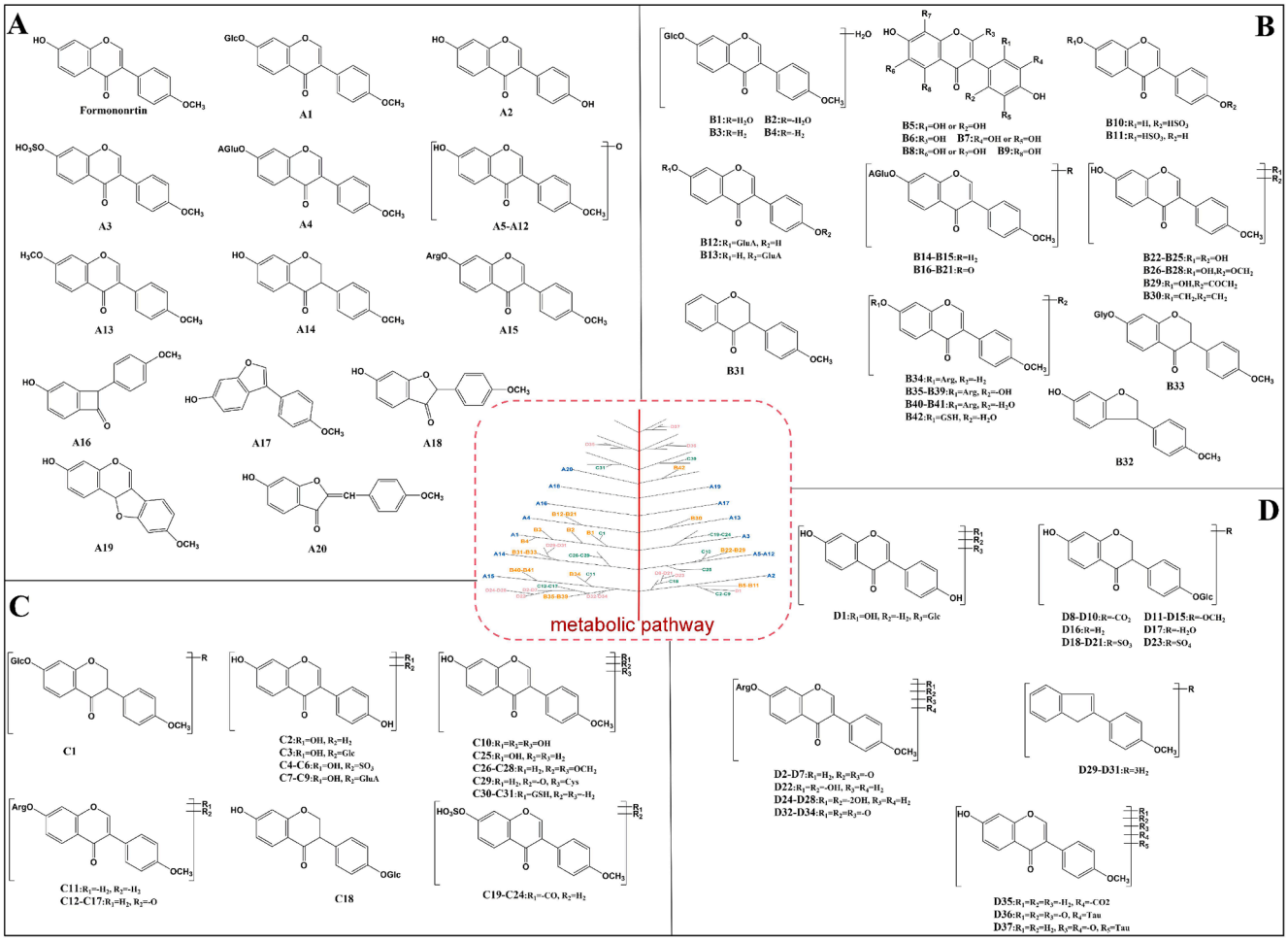

Fig. 3. Structural identification and proposed metabolic pathway of formononetin metabolites. A: primary branching metabolites of formononetin (A1-A20); B: secondary branching metabolites of formononetin (B1-B42); C: tertiary branching metabolites of formononetin (C1-C31); D: Multi-level branching metabolites of formononetin (D1-D37).

predicted using the Swiss Target Database. NAFLD-related targets were then searched for in the GeneCards database by using the term "non-alcoholic fatty liver disease". Finally, the targets of formononetin and its primary branch metabolites and NAFLD were mapped by Venny 2.1 software to screen for overlapping targets.

2.7.2. Construction of protein–protein interaction (PPI) network

Overlapping targets were analyzed with the String Version 11.0 platform to establish relationships between target proteins. The PPI network diagram was constructed using Cytoscape 3.9.1 for topological analysis. Core targets in the network were visualized based on degree values.

2.7.3. Biological function and pathway enrichment analyses

Using the Metascape database, the top 20 relevant biological processes and KEGG pathways were selected as key pathways for the main targets of formononetin and its primary branch metabolites for the treatment of NAFLD.

2.7.4. Construction of disease-pathways-targets-metabolites network

Diseases, major pathways, metabolites and key targets were linked together using Cytoscape 3.9.1 software. Visual analysis was performed by adjusting parameters. The disease-pathways-targets-metabolites network diagram was constructed to visually express their interactions.

2.8. Statistical analysis

Cell experiments were repeated at least three times. GraphPad Prism 8.0 was used to analyze the results of biochemical indices and related graphs. Two-tailed Student's *t*-test was used for statistical analysis. $P < 0.05$ was considered significant.

3. Results

3.1. The establishment of a recursive tree-based analytical strategy

We focused on a "recursive tree" analysis strategy to systematically screen and characterize the metabolites of drugs, using formononetin as an example (Fig. 1). Firstly, we defined the concept of "recursive tree". The drug is compared to a tree trunk, the metabolites resulting from the addition or subtraction of a single functional group are the primary branches (main branches), the metabolites resulting from the addition or subtraction of a single functional group from the primary branches are the secondary branches (lateral branches), and so on. Among the addition and subtraction of a single functional group include methylation (demethylation), hydroxylation (dehydroxylation), hydrogenation (dehydrogenation), methoxylation (demethoxylation), decarbonylation, decarbonization, *etc*. During the recursion process, two noteworthy points aroused our interest. One was the emergence of duplicate metabolites as the recursion progresses, and it was essential to remove duplicate metabolites when summarizing. Secondly, after the screening

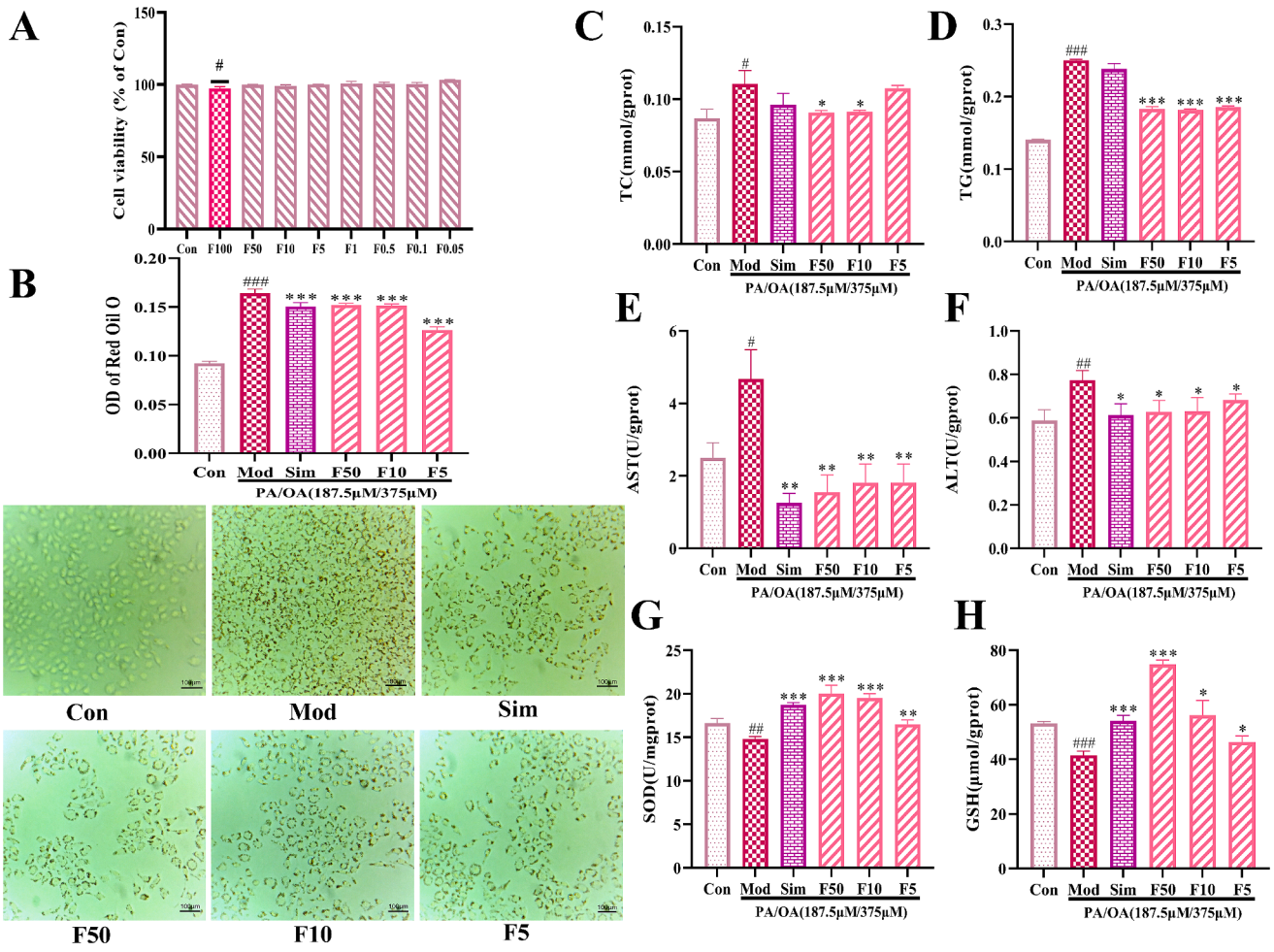

Fig. 4. Effects of formononetin on NAFLD cell models. (A) Results of cell viability; (B) Results of Oil Red O staining (×200); (C–H) Results of TG, TC, AST, ALT, SOD, and GSH levels. $^{\#}P < 0.05$, $^{\#\#}P < 0.01$, $^{\#\#\#}P < 0.001$ vs the Con group; $^{*}P < 0.05$, $^{**}P < 0.01$, $^{***}P < 0.001$ vs the Mod group.

of the tertiary branching metabolites, fewer and fewer metabolites could be identified, so we mainly performed the identification of the primary, secondary, and tertiary branching metabolites.

Not to be ignored, the diagnostic product ions (DPIs) played a key role in the "recursive tree" analysis strategy. The structural backbone of the prototype drug is largely preserved during metabolism, thus allowing rapid and precise structural identification of the metabolite using DPIs based on the mass fragmentation behavior of atomoxetine. In addition, the seamless integration of primary branching metabolites, which are used as effective forms of drugs due to their higher blood concentrations and well-defined structural formulas, with network pharmacology is key to the application of "recursive tree" analysis strategies.

3.2. Dpis construction based on formononetin mass cleavage pattern

Formononetin belongs to the class of isoflavones, and the DPIs are mainly produced by cleavage at different positions on the C-ring. It includes Retro-Diels-Alder (RDA) cleavage, deA-ring cleavage, and deB-ring cleavage, often accompanied by neutral loss of CO_2, CO, and H_2O. The prototype with the chemical formula $C_{16}H_{12}O_5$ was rapidly identified based on the retention time of formononetin standard at 9.65 min and the ions at *m/z* 267.06 ($[M-H]^-$) and *m/z* 269.08 ($[M+H]^+$). In order to more conveniently analyze the metabolites of formononetin, we list its six cleavage pathways (Fig. 2). In the negative ion mode, four typical ions with *m/z* 251, *m/z* 239, *m/z* 223, and *m/z* 209 were obtained after the sequential loss of O, CO, CO_2, and CH_2, respectively. Three characteristic ions with *m/z* 252, 236, and 208 were generated after the successive loss of CH_3, OCH_3, and CO, respectively. Moreover, six product ions were observed at *m/z* 107, 159, 146, 120, 135, and 132 through the cleavage pathway (a)\(b)\(c). Among them, *m/z* 135 and *m/z* 132 were typical RDA cleavage ions. According to the cleavage pathways (d)\(e)\(f), the ions were produced at *m/z* 119, 147, 91, 175, 159, and 107. Among them, *m/z* 91 and *m/z* 175 were the key ions of flavonoid cleavage mode II, and the product ion with high abundance at *m/z* 161 was produced by demethylation of *m/z* 175. Thus, the DPIs of formononetin were summarized as *m/z* 91, 107, 119, 120, 132, 135, 146, 147, 159, 175, 208, 209, 223, 236, 239, 251, 252 in negative ion mode. Similarly, the DPIs in positive ion mode were *m/z* 93, 109, 121, 122, 134, 137, 148, 149, 161, 177, 210, 211, 225, 238, 241, 253, 254.

3.3. Dpis construction of primary, secondary, tertiary, and multi-level branching metabolites

Based on the "recursive tree" analysis strategy and the general rules of drug metabolism, formononetin was susceptible to methylation (demethylation), oxidation (deoxidation), glucuronidation, sulfation, and their composite reactions. With the addition or subtraction of a single functional group in the parent nucleus as the core of the analysis strategy, we classified these metabolites into primary, secondary, tertiary, and multi-level branching metabolites, which resulted in the generation of regular DPIs. For example, daidzein, a demethylated metabolite of formononetin (primary branching metabolite), might yield negative ions at *m/z* 253 (*m/z* 267 - CH_2), *m/z* 237 (*m/z* 251 - CH_2),

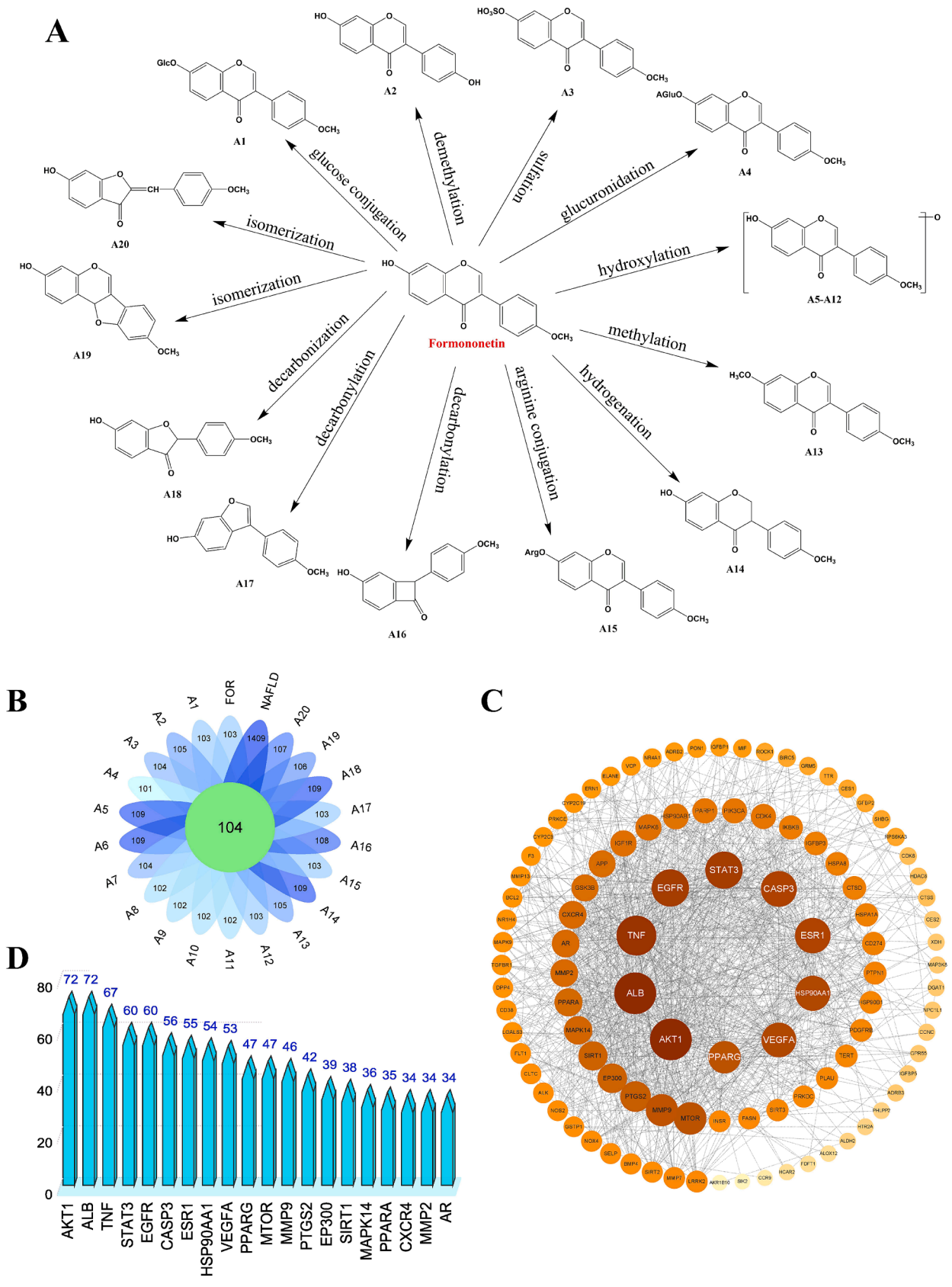

Fig. 5. (A) Metabolic process of the primary branching metabolites of formononetin; (B) Common targets of NAFLD and 21 metabolite targets (including formononetin); (C) PPI network diagram; (D) The 20 targets with the highest degree valu.

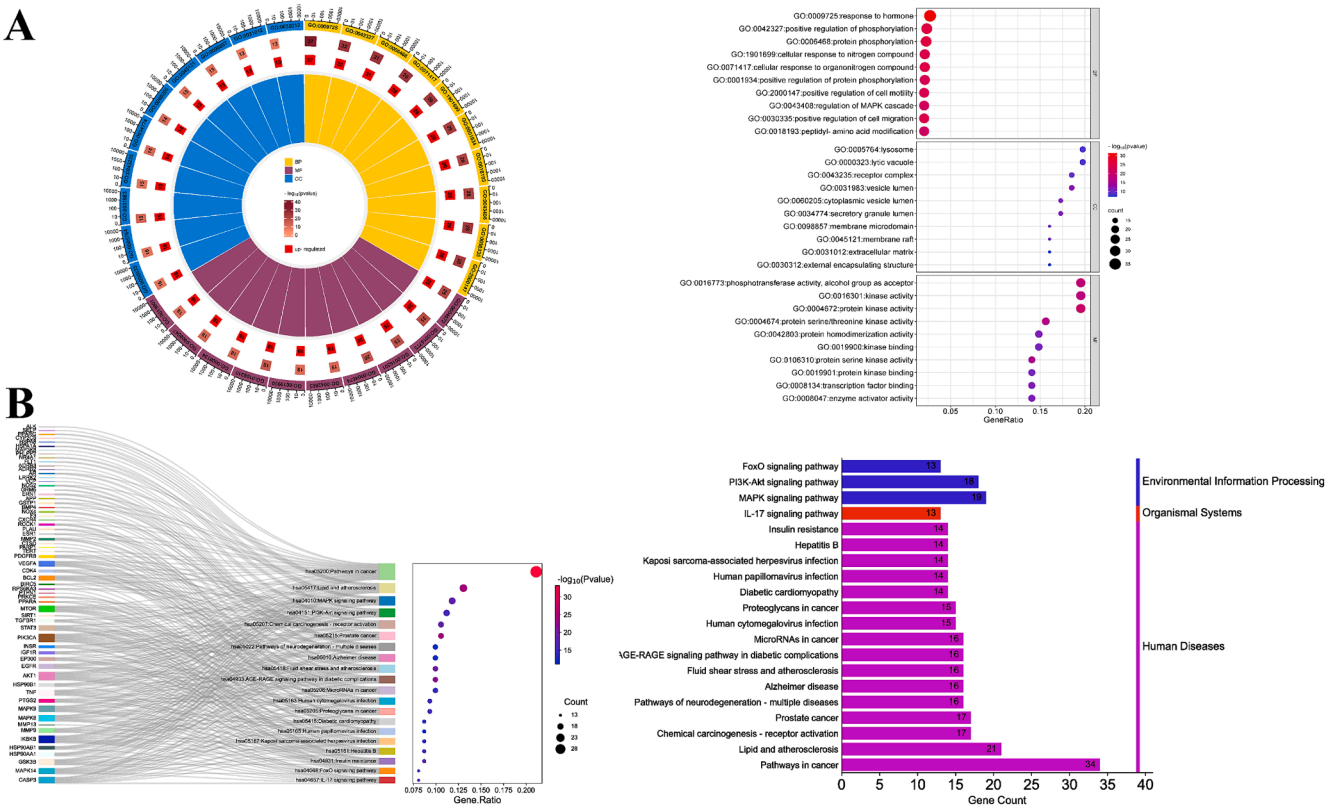

Fig. 6. (A) Circle and dot bubble plots for GO analysis; (B) Sankey dot and category summary plots for KEGG.

m/z 215 (*m/z* 239 - CH_2), *m/z* 209 (*m/z* 223 - CH_2), *m/z* 145 (*m/z* 159 - CH_2), *m/z* 118 (*m/z* 132 - CH_2), *m/z* 161 (*m/z* 175 - CH_2), and *m/z* 93 (*m/z* 107 - CH_2). Another one, glucuronidation metabolites of daidzein (secondary branching metabolite) might produce negative ions at *m/z* 429 (*m/z* 253 + GluA), *m/z* 413 (*m/z* 237 + GluA), *m/z* 391 (*m/z* 215 + GluA), *m/z* 385 (*m/z* 209 + GluA), *m/z* 321 (*m/z* 145 + GluA), *m/z* 294 (*m/z* 118 + GluA), *m/z* 337 (*m/z* 161 + GluA), and *m/z* 269 (*m/z* 93 + GluA). By analogy, the DPIs ± nX [n indicated the presence of multiple functional groups, X indicated molecular weight of substituents, *e.g.* 14 (CH_2), 16 (O), 18 (H_2O), 30 (OCH_2), 80 (SO_3), 176 (GluA), *etc.*] could be used to identify formononetin metabolites if multi-level branching reactions occurred.

3.4. Identification of formononetin metabolites

This study identified 131 metabolites of formononetin, with 53, 27, 46, 9, and 31 metabolites detected in plasma, urine, faeces, liver, and liver microsomes samples, respectively. Based on the "recursive tree" analysis strategy, we divided the metabolites into four groups, including primary, secondary, tertiary, and multi-level branching metabolites group. Table 1 provided detailed information on the formononetin metabolites. Fig. 3 illustrated the structure of the metabolites. Representative metabolites of formononetin were listed and the identification analysis of all metabolites was detailed in the **Supplementary Material**.

3.4.1. Representative primary branching metabolites of formononetin (A1-A20)

The retention time of **A1** in the positive ion mode was 6.92 min. Its theoretical $[M + H]^+$ ion at 431.13365 ($C_{22}H_{23}O_9$, mass error within ± 5 ppm), which was 162 Da greater than that of formononetin. In ESI-MS^2 spectrum, the fragment ions at *m/z* 269.08 $[M + H\text{-Glc}]^+$, *m/z* 253.05 $[M + H\text{-Glc-}CH_2]^+$, and *m/z* 237.06 $[M + H\text{-Glc-}OCH_2]^+$ were observed. Additionally, the DPIs of formononetin at *m/z* 107.09, *m/z* 136.06, and *m/z* 161.85 were also detected. It was inferred from the literature that **A1** was ononin (Li et al., 2020).

A2 yielded significant $[M-H]^-$/ $[M + H]^+$ ions at 253.05043 ($C_{15}H_9O_4$, mass error of −0.799 ppm) and *m/z* 255.06427 ($C_{15}H_{11}O_4$, mass error of −0.915 ppm) in negative and positive ion modes, respectively. It was 14 Da less massive than formononetin. And then, the fragment ions at *m/z* 237.06 $[M-H-O]^-$, *m/z* 225.06 $[M-H-CO]^-$, *m/z* 221.07 $[M-H-2O]^-$, and *m/z* 209.07 $[M-H-CO_2]^-$ were produced by a series of neutral losses of O, CO, and CO_2. These fragment ions confirmed that **A2** was the demethylated metabolite of formononetin, daidzein.

The $[M-H]^-$ ions of **A3**, **A4,** and **A15** were found at *m/z* 347.02319 ($C_{16}H_{11}O_7S$, mass error of 0.269 ppm), *m/z* 443.09888 ($C_{22}H_{19}O_{10}$, mass error of 0.045 ppm), and *m/z* 423.16559 ($C_{22}H_{23}N_4O_5$, mass error of −1.261 ppm). **A3**, **A4,** and **A15** were 80 Da, 176 Da, and 156 Da larger than that of formononetin, respectively, suggesting that **A3**, **A4,** and **A15** could be deduced to be sulfated metabolite, glucuronidated metabolite and arginine conjugated metabolite of formononetin, respectively. In their ESI-MS^2 spectra, the significant fragment ion at *m/z* 267.06 was formed by the neutral loss of SO_3, GluA, and Arg, respectively. Other DPIs of formononetin at *m/z* 91.06, *m/z* 107.09, *m/z* 135.05, *m/z* 147.06, *m/z* 209.03, *m/z* 223.85, and *m/z* 252.05 were observed. Therefore, **A3**, **A4**, and **A15** were deduced as formononetin-7-O-sulfate, formononetin-7-O-GluA, and formononetin-7-O-Arg, respectively.

Eight isomeric metabolites, **A5-A12** were 16 Da more massive than formononetin, and their theoretical $[M-H]^-$/$[M + H]^+$ ions at *m/z* 283.06009 ($C_{16}H_{11}O_5$, mass errors within ± 5 ppm) and *m/z* 285.07575 ($C_{16}H_{13}O_5$, mass errors within ± 5 ppm). Therefore, **A5-A12** were initially identified as the mono-hydroxylated metabolites of formononetin. Among them, the MS^2 spectra of **A5-A9** all showed complementary fragment ions at *m/z* 135.01 ($C_7H_3O_3$) and *m/z* 147.04 ($C_9H_7O_2$), which were generated by cleavage pathway (c), indicating hydroxylation in the B-ring or C-ring. Notably, the pathway cleavage (b) of **A7** produced fragment ions at *m/z* 163.00 ($C_8H_3O_4$) and *m/z* 120.06

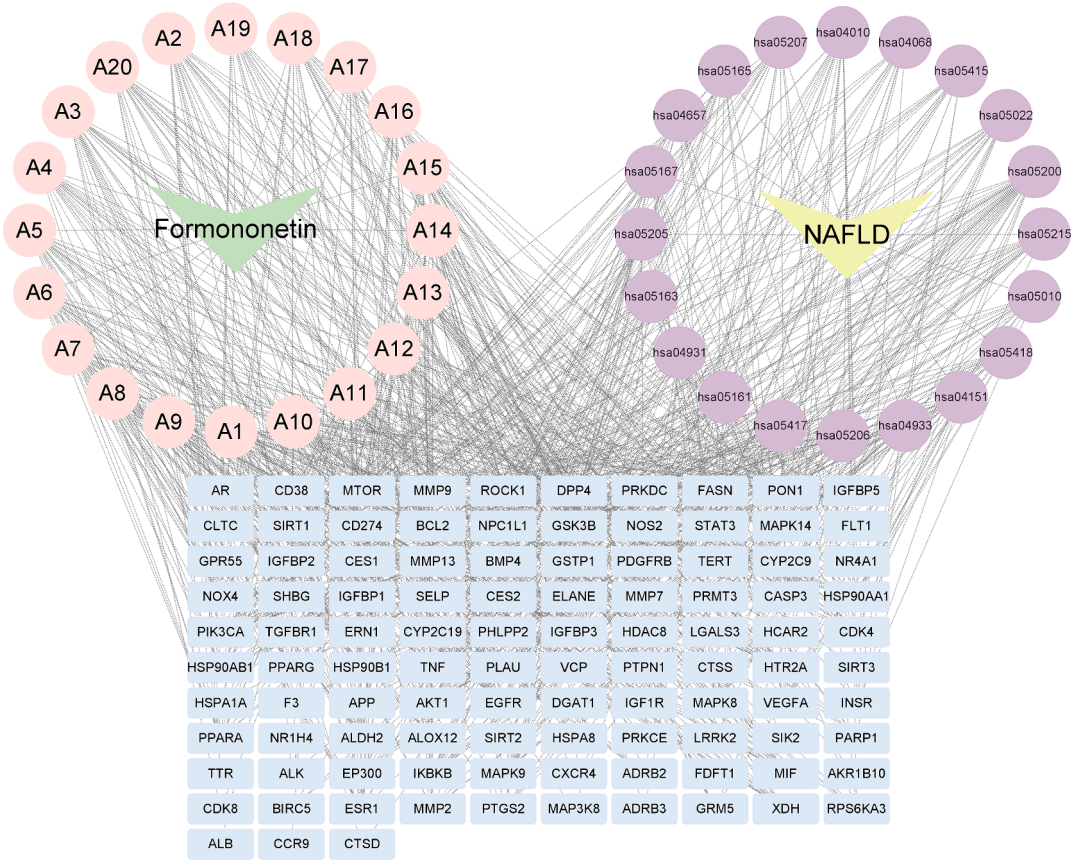

Fig. 7. Disease-Pathways-Targets-Metabolites Network Diagram. Note: yellow triangles: NAFLD; Green triangles: formononetin; Purple circles: pathways; Pink circles: primary branching metabolites of formononetin; Baby blue quadrilaterals: targets.

(C_8H_8O), indicating hydroxylation in the C-2 position. In general, the larger the Clog*P* value, the longer the retention time. Clog*P* values for the substituted hydroxyl groups of C-2′, C-6′, C-3′, and C-5′ were 1.11784, 1.11784, 1.48784, and 1.48784, respectively. Therefore, the hydroxyl substitution of C-2′ and C-6′ were **A5** and **A6** (or **A6** and **A5**), and the hydroxyl substitution of C-3′ and C-5′ were **A8** and **A9** (or **A9** and **A8**). Furthermore, **A10**, **A11**, and **A12** all showed fragment ions at *m/z* 152.01 ($C_7H_4O_4$) and *m/z* 132.06 (C_9H_8O), which were typical DPIs generated by RDA cleavage. The *m/z* 152.01 indicated the presence of two hydroxyl groups in the A-ring. This was also confirmed by the ions at *m/z* 136.06, *m/z* 114, *m/z* 91.06, and *m/z* 71.00 produced by the cleavage pathway (c)/(e). In other words, the hydroxyl substitution in the A-ring has three positions: C-5, C-6, and C-8. The hydroxyl group in the C-5 position readily formed an intramolecular hydrogen bond with the carbonyl group in the C-4 position, thus greatly reduced the polarity of the metabolite and its retention time. It was deduced that **A12** was 5-hydroxyl-formononetin (Biochanin A). The Clog*P* values of **A10** and **A11** were both 1.57529, so it was difficult to distinguish between C-6 and C-8 substituted hydroxyl groups.

3.4.2. Representative secondary branching metabolites of formononetin (B1-B42)

B1 produced $[M-H]^-$ ion with a mass of *m/z* 447.13028 ($C_{22}H_{23}O_{10}$, mass error of 1.364 ppm), which was 18 Da more than **A1**. In the ESI-MS^2 spectrum, the fragment ions at *m/z* 429.12 $[M-H-H_2O]^-$ and *m/z* 202.80 $[M-H-H_2O-Glc-CO_2-OCH_3]^-$ were generated. Other DPIs were found at *m/z* 175.00, *m/z* 135.01, and *m/z* 121.06. Thus, **B1** was a secondary branching metabolite resulting from the hydrolysis of **A1**.

Five isomeric metabolites, **B5-B9** were 14 Da less massive than **A5-A12**. And thus,

they were tentatively inferred to be demethylated products of **A5-A12**. In their ESI-MS^2 spectra, the DPIs at *m/z* 251.05 $[M-H-O]^-$, *m/z* 241.88 $[M-H-CO]^-$, and *m/z* 225.06 $[M-H-CO_2]^-$ were obtained after the sequential loss of O, CO, and CO_2, respectively. Based on the structural characteristics of **A5-A12** and the Clog*P* values, the structures of **B5-B9** were inferred (Fig. 3).

B10 and **B11** afforded $[M-H]^-$ ion at *m/z* 333.00634 ($C_{15}H_9O_7S$, mass errors within ± 5 ppm), which were 80 Da more massive than **A2**. The product ions of **B10** and **B11** at *m/z* 305.86 $[M-H-CO]^-$ and *m/z* 253.05 $[M-H-SO_3]^-$ were observed. Furthermore., the ions of *m/z* 135.05 and *m/z* 117.93 (*m/z* 198-SO_3) were generated in **B10**; *m/z* 214.88 and *m/z* 217.87 were generated in **B11**. The Clog*P* values for **B10** and **B11** were 0.4985 and 0.879, respectively. Therefore, **B10** was daidzin-4′-O-sulfate, **B11** was daidzin-7-O-sulfate.

The retention times of **B12** and **B13** were 4.66 and 5.31 min, respectively, with a mass 14 Da smaller than that of **A4**, and the $[M-H]^-$ ions produced in the negative ion mode were *m/z* 429.08377 and *m/z* 429.08231 ($C_{21}H_{17}O_{10}$, mass errors within ± 5 ppm). Therefore, both **B12** and **B13** were deduced as glucuronidation and demethylation metabolites of formononetin. *M/z* 117.93 and *m/z* 293.80 (117 + GluA) were B-ring fragment ions produced by RDA cleavage of **B12** and **B13**, respectively. It was determined that **B12** was daidzin-7-O-GluA and **B13** was daidzin-4′-O-GluA.

3.4.3. Representative tertiary branching metabolites of formononetin (C1-C31)

C1 showed theoretical deprotonated molecular ion at *m/z* 449.14703 ($C_{22}H_{25}O_{10}$, mass error of 1.807 ppm), which was 2 Da more massive than **B1**. Two predominant fragment ions at *m/z* 405.30 $[M-H-CO-H_2O]^-$ and *m/z* 374.43 $[M-H-CO_2-H_2O-CH_3]^-$ were detected. Additionally, high abundance ions at *m/z* 447.14 (**B1**) and *m/z* 431.11 (**B1**-O) were generated. Based on this, **C1** was identified as the

Table 1a
Primary branching metabolites of formononetin **(A1-A20)**.

A15	N	8.05	$C_{22}H_{23}N_4O_5$	423.16629	423.16559	13.5	−1.261	269(100),304(93),205(90),178(81),423(15)	-	-	-	+	+	-	-
A16	P	6.43	$C_{15}H_{13}O_3$	241.08592	241.08516	9.5	−0.750	241(100),107(49),131(30),119(2),93(2)	−	−	−	−	+	−	+
A17	P	7.89	$C_{15}H_{13}O_3$	241.08592	241.08516	9.5	−3.156	109(100),241(9),131(5),147(2),95(2)	−	−	−	−	+	−	+
A18	P	5.52	$C_{15}H_{13}O_4$	257.08083	257.08005	9.5	−0.785	123(100),257(62),137(12),107(24),121(3)	+	+	−	−	−	−	−
A19	N	8.29	$C_{16}H_{11}O_4$	267.06519	267.06635	11.5	4.211	252(100),267(87),220(5),59(5),161(2)	+	+	+	−	−	−	−
A20	N	6.99	$C_{16}H_{11}O_4$	267.06519	267.06631	11.5	4.211	252(100),267(96),220(6),201(4),132(2)	+	+	+	+	−	−	−

hydrogenated metabolite of **B1**, a tertiary branching metabolite of formononetin.

C2 generated its $[M-H]^-$ ion at *m/z* 271.06100 ($C_{15}H_{11}O_5$, mass error of 0.132 ppm) with the retention time of 7.20 min. It was 2 Da more massive than **B5-B9**, extrapolating that **C2** was a hydrogenated metabolite of **B1**. The DPIs at *m/z* 251.05, *m/z* 241.88, and *m/z* 225.06 were observed. **C3** afforded the deprotonated molecular ion at *m/z* 431.09869 ($C_{21}H_{19}O_{10}$, mass error of 0.320 ppm) with a mass 162 Da larger than that of **B5-B9**, and generated fragment ions at *m/z* 269.08 $[M-H-Glc]^-$, *m/z* 255.05 $[M-H-Glc-CH_2]^-$, *m/z* 241.88 $[M-H-Glc-CO]^-$, and *m/z* 225.06 $[M-H-Glc-CO_2]^-$. Hence, **C3** was characterized as a glucosylation product of **B5-B9**. Moreover, **C4-C6** has the same theoretical $[M-H]^-$ ion at *m/z* 349.00238 ($C_{15}H_9O_8S$, mass errors within ± 5 ppm), which were 80 Da more massive than **B5-B9**. The fragment ions at *m/z* 269.08 $[M-H-SO_3]^-$, *m/z* 241.88 $[M-H-SO_3-CO]^-$, and *m/z* 225.06 $[M-H-CO_2]^-$ were exhibited. So, **C4-C6** were speculated to be sulfated metabolites of **B5-B9**. Similarly, the dominant ion at *m/z* 269.08 $[M-H-GluA]^-$ was detected in the ESI-MS^2 spectra of **C7-C9**. They were 176 Da more massive than **B5-B9**, inferring that they were glucuronided metabolites of **B5-B9**.

3.4.4. Representative mmulti-level branching metabolites of formononetin (D1-D37)

D1 had $[M-H]^-$ ion at *m/z* 433.11414 ($C_{21}H_{21}O_{10}$, mass error of 0.120 ppm) in the ESI-MS^2 spectrum. It was 2 Da less massive than **C3**. Besides, glucosylation reaction characterization was presented. The fragment ions at *m/z* 415.43 $[M-H-H_2O]^-$, *m/z* 271.05 $[M-H-Glc]^-$, *m/z* 257.08 $[M-H-Glc-CH_2]^-$, and *m/z* 239.06 $[M-H-Glc-CH_2-H_2O]^-$ were presented. Based on the analysis above, **D1** was a dehydrogenated metabolite of **C3**. However, it could be clearly stated that demethylation occurred at the C-4′ position.

D2-D7 with experimental $[M-H]^-$ ion at *m/z* 393.19211 ($C_{22}H_{25}N_4O_3$, mass errors within ± 5 ppm) were observed. They were 16 Da less massive than **C12-C17**, suggesting that **D2-D7** were the deoxygenated products of **C12-C17**. Noteworthy ions at *m/z* 133.45 and *m/z* 104.07 (260-Arg) from RDA cleavage, and fragment ions at *m/z* 147.04 and *m/z* 246.00 from cleavage pathway (e), suggesting that arginine conjugation occurred in the C-7 position and two oxygen deletions in the C-ring, with hydrogenation of C-2 and C-3. Moreover, **D22**, **D24-D28**, and **D32-D34** were also arginine conjugation metabolites with only a few structural changes. Their structures were predicted based on the results of fragment ions analysis and the DPIs of the primary and secondary branching arginine conjugation metabolites, as shown in Fig. 3. They were all defined as multi-level branching metabolites of formononetin.

3.5. Effects of formononetin on HepG2 cells induced by PA/OA

Literatures reported that PA/OA stimulation of HepG2 cells can mimic fatty hepatocytes for NAFLD studies. We successfully established a NAFLD cell model by stimulating HepG2 cells with PA (187.5 μM) / OA (375 μM). The effect of formononetin on HepG2 cells viability was assessed by CCK-8, and the results showed that cells viability was significantly reduced at formononetin concentrations greater than 100 $\mu g \cdot mL^{-1}$ (Fig. 4A). To ensure the anti-NAFLD efficacy of formononetin, the concentrations of 5, 10, and 50 $\mu g \cdot mL^{-1}$ were selected for subsequent experiments.

After 24 h of PA/OA stimulation, HepG2 cells showed severe lipid accumulation. However, the number of lipid droplets in the cells was significantly reduced after formononetin treatment (Fig. 4B), and the levels of TC and TG decreased, indicating that formononetin has a lipid-lowering effect (Fig. 4C, D). At the same time, the levels of AST and ALT were also significantly reduced (Fig. 4E, F), indicating that formononetin has hepatoprotective effects. Moreover, lipid accumulation easily leads to oxidative stress. Formononetin dose-dependently reversed the PA/OA-induced increase in SOD levels and decrease in GSH levels (Fig. 4G**,** **H**). Our data preliminarily demonstrated the ameliorative effect of formononetin in NAFLD.

3.6. Network pharmacology analysis

Primary branching metabolites play an important role in drug metabolism because they retain similar parent nucleus structures (Li et al., 2009). Moreover, in our study, the structures of the primary branching metabolites of formononetin were completely characterized. Therefore, we selected formononetin and its primary branching metabolites for a network pharmacological analysis to explore the mechanism of anti-NAFLD.

3.6.1. Relevant targets of formononetin and primary branching metabolites against NAFLD

Fig. 5A illustrates the metabolic process of the primary branching metabolites of formononetin. The targets of 21 (including formononetin) metabolites were gathered from the Swiss Target Prediction database, and a total of 566 targets were obtained after removing duplicate targets. Additionally, using the GeneCards database, 1409 targets associated with NAFLD were acquired. Through Venny 2.1 software, the metabolites and NAFLD targets were overlapped, and 104 common target genes were determined (Fig. 5B).

3.6.2. Analysis of PPI network

These 104 candidate targets were entered into Cytoscape 3.9.1 software and a PPI network with 104 nodes and 1046 edges was constructed. Notably, we chose orange dots to represent nodes with higher degree values. They were more influential in the mechanism of formononetin anti-NAFLD (Fig. 5C). The top 20 targets with the highest degree values were listed in Fig. 5D, including AKT1, ALB, TNF, STAT3, EGFR, *etc*.

3.6.3. GO and KEGG enrichment analysis

GO functional annotation and KEGG pathway enrichment were performed on 104 targets using the Metascape database. The top 10 enriched BP (biological process), MF (molecular function), and CC (cellular compound) were graphically analyzed (Fig. 6A). BP was mainly involved in response to the hormone, positive regulation of phosphorylation, protein phosphorylation, and cellular response to the organonitrogen compound. MF was mainly involved in protein kinase activity, phosphotransferase activity, alcohol group as acceptor, kinase activity, and protein serine/threonine kinase activity. CC was mainly involved in the lytic vacuole, lysosome, vesicle lumen, and receptor complex. KEGG enrichment analysis showed that many targets in pathways in cancer, lipid and atherosclerosis, and MAPK signaling pathways were enriched.

Table 1b
Secondary branching metabolites of formononetin **(B1-B42)**.

ID	Ion Mode	t_R/ min	Formula $[M-H]^-$/ $[M+H]^+$	Theoretical Mass (*m/z*)	Experimental Mass (*m/z*)	RDB	Error (ppm)	MS/MS Fragment Ions	PS	PM	PA	U	F	L	LM
B1 (A1)	N	6.54	$C_{22}H_{23}O_{10}$	447.12857	447.13028	11.5	1.364	201(100),447(65),113(63),85(37),175(21)	–	–	–	+	–	–	–
	P	6.53	$C_{22}H_{25}O_{10}$	449.14422	449.14743	10.5	3.207	393(100),337(68),83(45),449(30),57(22)	–	–	–	–	–	+	–
B2 (A1)	N	4.31	$C_{22}H_{19}O_8$	411.10744	411.10733	13.5	−2.945	255(100),375(68),212(15),411(12),184(1)	–	–	–	–	–	+	–
B3 (A1)	N	8.82	$C_{22}H_{23}O_9$	431.13365	431.13458	11.5	−0.407	113(100),431(70),85(57),121(38),255(34)	–	–	–	+	–	–	–
B4 (A1)	P	9.21	$C_{22}H_{21}O_9$	429.11800	429.11685	12.5	−1.159	429(100),193(58),149(31),237(31),385(21)	+	+	+	–	–	–	+
B5 (A2)	N	5.72	$C_{15}H_9O_5$	269.04444	269.04550	11.5	−0.173	269(100),225(14),169(10),241(8),121(2)	–	–	–	–	–	–	+
	P	5.70	$C_{15}H_{11}O_5$	271.06009	271.05908	10.5	−2.123	271(100),215(9),197(4),136(2),153(2)	–	–	–	–	–	–	+
B6 (A2)	N	6.25	$C_{15}H_9O_5$	269.04444	269.04565	11.5	0.384	269(100),253(32),225(2),209(8),173(1)	+	–	–	–	–	–	+
	P	6.25	$C_{15}H_{11}O_5$	271.06009	271.05948	10.5	−0.620	271(100),255(60),197(12),136(2),79(1)	+	–	–	–	–	–	+
B7 (A2)	N	6.43	$C_{15}H_9O_5$	269.04444	269.04544	11.5	−0.396	269(100),213(2),225(2),197(2),173(1)	–	–	–	–	–	–	+
	P	6.44	$C_{15}H_{11}O_5$	271.06009	271.05902	10.5	−3.984	271(100),215(6),197(3),153(2),136(0.4)	–	–	–	–	–	–	+
B8 (A2)	N	6.61	$C_{15}H_9O_5$	269.04444	269.04553	11.5	−0.062	269(100),225(3),240(2),197.06(1),69(1)	–	–	–	–	–	–	+
	P	6.62	$C_{15}H_{11}O_5$	271.06009	271.05917	10.5	−3.431	271.06(100),215(6),136(4),197(2),153(2)	–	–	–	–	–	–	+
B9 (A2)	N	8.39	$C_{15}H_9O_5$	269.04444	269.04581	11.5	0.979	269(100),253(41),225(20),59(9),197(9)	+	–	–	–	–	–	–
	P	8.40	$C_{15}H_{11}O_5$	271.06009	271.05917	10.5	−3.431	271(100),167(6),153(5),215(4),253(1)	–	–	–	+	–	–	–
B10 (A2)	N	4.19	$C_{15}H_9O_7S$	333.00634	333.00742	11.5	−0.027	214(4),253(79),333(43),81(27),305(2)	+	–	–	–	–	–	–
B11 (A2)	N	5.97	$C_{15}H_9O_7S$	333.00634	333.00766	11.5	0.213	253(100),333(37),80(2),32(1),130(1)	+	–	–	–	–	–	–
	P	5.98	$C_{15}H_{11}O_7S$	335.02199	335.02109	10.5	−0.910	255(100),335(30),199(4),117(2),184(2)	+	+	–	+	–	–	–
B12 (A4)	N	4.66	$C_{21}H_{17}O_{10}$	429.08162	429.08377	13.5	2.447	253(100),113(42),85(21),175(19),429(10)	+	+	+	–	–	–	–
	P	4.65	$C_{21}H_{19}O_{10}$	431.09727	431.09631	12.5	−0.963	255(100),98(12),421(9),178(5),348(3)	+	+	+	+	–	–	–
B13 (A4)	N	5.31	$C_{21}H_{17}O_{10}$	429.08162	429.08231	13.5	−0.955	253(100),113(84),85(44),429(42),175(32)	+	+	+	–	–	–	–
	P	5.30	$C_{21}H_{19}O_{10}$	431.09727	431.09625	12.5	−1.023	255(100),431(12),85(3),70(2),199(2)	+	+	+	–	–	–	–
B14 (A4)	N	8.86	$C_{22}H_{21}O_{10}$	445.11292	445.11426	12.5	0.539	121(100),445(84),225(51),181(34),357(24)	+	+	+	–	–	–	+
B15 (A4)	N	7.24	$C_{22}H_{21}O_{10}$	445.11292	445.11523	12.5	2.718	269(100),113(71),175(35),85(33),445(17)	+	+	+	–	–	–	–
	P	7.23	$C_{22}H_{23}O_{10}$	447.12857	447.12518	11.5	−3.393	271(100),137(59),163(56),121(9),109(8)	+	–	+	–	–	–	–
B16 (A4)	N	4.79	$C_{22}H_{19}O_{11}$	459.09218	459.09381	13.5	1.144	283(100),267(24),241(16),173(11),83(8)	+	+	+	–	–	–	–
	P	4.79	$C_{22}H_{21}O_{11}$	461.10783	461.10519	12.5	−2.648	285(100),269(94),113(66),85(32),175(28)	+	+	+	+	–	–	–
B17 (A4)	N	5.98	$C_{22}H_{19}O_{11}$	459.09218	459.09399	13.5	1.537	268(100),459(92),283(53),113(47),85(38)	+	–	–	–	–	–	–
B18 (A4)	N	6.84	$C_{22}H_{19}O_{11}$	459.09218	459.09409	13.5	1.754	283(100),268(25),459(10),87(5),175(5)	–	–	–	–	–	–	+
	P	6.81	$C_{22}H_{21}O_{11}$	461.10783	461.10611	12.5	−3.747	284(100),461(83),255(9),136(3),89(1)	–	–	–	–	–	–	+
B19 (A4)	P	7.03	$C_{22}H_{21}O_{11}$	461.10783	461.10614	12.5	−3.682	284(100),461(60),126(9),337(5),136(4)	–	–	–	–	–	–	+
B20 (A4)	N	7.46	$C_{22}H_{19}O_{11}$	459.09218	459.09390	13.5	1.341	283(100),459(41),268(37),113(3),69(3)	+	+	+	–	–	–	–
	P	7.48	$C_{22}H_{21}O_{11}$	461.10783	461.10660	12.5	−1.238	114(100),99(70),136(42),159(38),142(27)	+	–	–	–	–	–	–
B21 (A4)	N	9.54	$C_{22}H_{19}O_{11}$	459.09218	459.09134	13.5	−1.945	121(100),401(79),313(57),225(14),459(6)	+	+	+	–	–	+	+
B22 (A5-A12)	N	6.06	$C_{16}H_{11}O_6$	299.05501	299.05603	11.5	−0.272	299(100),240(25),228(9),148(3),176(2)	–	–	–	–	–	–	+
	P	6.06	$C_{16}H_{13}O_6$	301.07066	301.06946	10.5	−4.001	301(100),286(20),241(7),268(7),152(4)	–	–	–	–	–	–	+

(*continued on next page*)

Table 1b (*continued*)

ID	Ion Mode	t_R/ min	Formula $[M-H]^-$/ $[M+H]^+$	Theoretical Mass (*m/z*)	Experimental Mass (*m/z*)	RDB	Error (ppm)	MS/MS Fragment Ions	PS	PM	PA	U	F	L	LM
B23 (A5-A12)	N	6.87	$C_{16}H_{11}O_6$	299.05501	299.05603	11.5	−0.372	284.03(100),140(15),256(5),148(4),176(1)	–	–	–	–	–	–	+
	P	6.88	$C_{16}H_{13}O_6$	301.07066	301.06943	10.5	−4.101	301(100),286(26),241(5),153(4),136(2)	–	–	–	–	–	–	+
B24 (A5-A12)	P	7.28	$C_{16}H_{13}O_6$	301.07066	301.07123	10.5	1.878	301(100),95(50),81(44),109(40),286(1)	–	–	–	–	+	–	–
B25 (A5-A12)	N	8.69	$C_{16}H_{11}O_6$	299.05501	299.05624	11.5	0.430	299(100),191(11),240(8),268(8),134(5)	–	–	–	–	–	–	+
B26 (A5-A12)	N	9.01	$C_{17}H_{13}O_5$	297.07575	297.07678	11.5	−0.225	297(100),268(82),224(21),134(15),196(2)	–	–	–	–	–	–	+
B27 (A5-A12)	P	9.73	$C_{17}H_{15}O_5$	299.09140	299.09073	10.5	−2.240	299(100),81(44),136(36.59),95(32),121.(30)	–	–	–	+	–	–	–
B28 (A5-A12)	N	9.84	$C_{17}H_{13}O_5$	297.07575	297.07669	11.5	−0.528	297(100),268(92),224(6),134(5),112(3)	–	–	–	–	–	–	+
B29 (A5-A12)	P	4.20	$C_{18}H_{15}O_6$	327.08631	327.08569	11.5	−1.910	208(100),182(88),327(39),169(29),110(13)	–	–	–	+	–	–	–
B30 (A13)	N	12.44	$C_{18}H_{15}O_4$	295.09648	295.09763	11.5	0.162	295(100),280(88),134(33),79(18),61(7)	–	–	–	–	–	–	+
	P	12.47	$C_{18}H_{17}O_4$	297.11213	297.11090	10.5	−4.158	297(100),270(4),81(3),95(3),137(2)	–	–	–	–	–	–	+
B31 (A14)	P	7.49	$C_{16}H_{15}O_3$	255.10157	255.10184	9.5	1.055	255(100),142(66),119(10),133(10),237(8)	–	–	–	+	–	–	–
B32 (A14)	P	6.18	$C_{15}H_{15}O_3$	243.10157	243.10086	8.5	−0.711	243(100),197(87),137(46),120(30),77(27)	+	+	+	+	–	–	–
B33 (A14)	P	7.99	$C_{18}H_{18}NO_5$	328.11794	328.11768	10.5	−0.820	328(100),152(3),130(3),198(2),286(2)	–	–	–	+	–	–	–
B34 (A15)	N	12.67	$C_{22}H_{21}N_4O_5$	421.15064	421.15543	14.5	0.687	421(100),221(78),136(32),96(21),77(10)	–	+	+	–	–	–	–
B35 (A15)	N	6.88	$C_{22}H_{23}N_4O_4$	407.17138	407.17310	13.5	1.526	407(100),80(90),96(23),61(22),325(14)	–	–	–	–	+	–	–
B36 (A15)	N	7.26	$C_{22}H_{23}N_4O_4$	407.17138	407.17346	13.5	2.411	407(100),80(10),343(9),392(7),96(6)	–	–	–	–	+	–	–
B37 (A15)	N	8.82	$C_{22}H_{23}N_4O_4$	407.17138	407.17203	13.5	−1.101	407(100),80(4),392(3),345(2),78(2)	–	–	–	–	+	–	–
B38 (A15)	N	9.19	$C_{22}H_{23}N_4O_4$	407.17138	407.17383	13.5	3.319	407(100),389(10),80(9),377(6),96(3)	–	–	–	–	+	–	–
B39 (A15)	N	9.23	$C_{22}H_{23}N_4O_4$	407.17138	407.17349	13.5	2.484	407(100),80(43),377(35),307(14),125(13)	–	–	–	–	+	–	–
B40 (A15)	P	3.73	$C_{22}H_{23}N_4O_4$	407.17138	407.17023	13.5	−1.152	377(45),407(86),349(35),307(19),125(9)	–	+	–	–	–	–	+
B41 (A15)	N	6.58	$C_{22}H_{21}N_4O_4$	405.15573	405.15845	14.5	4.002	80(100),405(73),96(19),124(13),171(12)	–	–	–	–	+	–	–
	P	6.54	$C_{22}H_{23}N_4O_4$	407.17138	407.17029	13.5	−1.092	201(100),407(72),330(40),130(29),348(13)	–	+	–	–	–	–	–
B42	N	9.45	$C_{26}H_{24}N_3O_8S$	538.12786	538.13043	16.5	2.734	538(100),421(100),389(10),330(40),221(16)	–	–	–	–	+	–	–

Fig. 6B provided the top 20 important signaling pathways.

3.6.4. *Building a "disease-pathways-targets-metabolites" network*

The "Disease-Pathway-Target-Metabolite" network diagram constructed by Cytoscape 3.9.1 software includes 20 pathways, 104 targets, 21 metabolites, and NAFLD. In the diagram, 20 primary branching metabolites were surrounded by formononetin as the center. With NAFLD as the center, 20 related pathways were encircled. Among them, NAFLD, formononetin, pathways, metabolites, and targets were represented by yellow triangles, green triangles, purple circles, pink circles, and baby blue quadrilaterals, respectively. Both metabolites and pathways were connected to the targets with lines (Fig. 7).

4. Discussion

4.1. *Feasibility analysis of recursive tree strategy establishment*

Metabolite identification is a crucial step in drug metabolism research, as well as the material basis for pharmacology and pharmacodynamics research. Drug metabolites have the characteristics of complex background matrix, diverse species, and low content, which require strong detection capability of their analytical instruments. LC-HRMS has become a powerful technical tool for the analysis of drug metabolite due to its high sensitivity, high accuracy, and high separation capacity (Cui et al., 2022). By combining various data processing methods, it can be used for the characterization of metabolites, as well as the detection and structural identification of unknown trace metabolites. However, the spectral information included in the existing chemical standards and databases is very limited, and the complex and diverse metabolite structure identification cannot be satisfied by LC-HRMS technology alone. Therefore, more new techniques and research strategies are needed to meet this challenge.

In the face of this bottleneck, we have proposed the first "recursive tree" analysis strategy. Based on the addition or subtraction of a single functional group, the metabolites were classified into primary, secondary, tertiary, and multi-level branching metabolites. Taking formononetin as an example, formononetin metabolites were identified and analyzed using the recursive tree analysis strategy *in vivo* and *in vitro*. A total of 131 metabolites were identified, of which 106 were detected *in vivo* and 31 were detected *in vitro*. From the identification results, the implementation of the recursive tree analysis strategy could expand the scope of metabolite search and obtain as many metabolites as possible. In addition, the use of the recursive tree strategy and the analysis of parameters in the mass spectrometry profiles ensure the

Table 1c
Tertiary branching metabolites of formononetin **(C1-C31)**.

ID	Ion Mode	t_R/ min	Formula $[M-H]^-$/ $[M+H]^+$	Theoretical Mass (*m/z*)	Experimental Mass (*m/z*)	RDB	Error (ppm)	MS/MS Fragment Ions	PS	PM	PA	U	F	L	LM
C1 (B1)	N	6.97	$C_{22}H_{25}O_{10}$	449.14422	449.14703	10.5	1.807	449(100),116(42),187 (20),374(2),405(2)	–	–	–	+	–	–	–
	P	6.96	$C_{22}H_{27}O_{10}$	451.15987	451.15942	9.5	−1.005	158(100),334(37),207 (27),120(22),451(11)	–	–	–	+	–	–	–
C2 (B5-B9)	N	7.20	$C_{15}H_{11}O_5$	271.06009	271.06100	11.5	0.132	271(100),252(100),221 (2),206(1),134(2),121(5)	–	–	–	–	–	–	+
C3 (B5-B9)	N	5.52	$C_{21}H_{19}O_{10}$	431.09727	431.09869	12.5	0.320	431(100),113(77),85 (48),255(47),149(43)	+	+	+	–	–	–	–
C4 (B5-B9)	N	4.97	$C_{15}H_9O_8S$	349.00126	349.00238	11.5	0.054	269(100),349(57),116 (3),190(3),80(2)	+	+	+	–	–	–	–
C5 (B5-B9)	N	6.96	$C_{15}H_9O_8S$	349.00126	349.00269	11.5	0.942	269(100),349(57),116 (3),190(3),80(2)	+	–	–	–	–	–	–
C6 (B5-B9)	N	4.79	$C_{15}H_9O_8S$	349.00126	349.00269	11.5	0.942	269(100),349(52),219(6),80 (4),62(4)	+	–	–	–	–	–	–
C7 (B5-B9)	N	4.42	$C_{21}H_{17}O_{11}$	445.07653	445.07703	13.5	−1.358	269(100),445(8),225(5),78 (5),134(3)	–	–	–	–	–	–	+
	P	4.40	$C_{21}H_{19}O_{11}$	447.09218	447.09030	12.5	−4.222	270(100),447(82),136 (12),241(7),70(6)	–	–	–	–	–	–	+
C8 (B5-B9)	N	5.93	$C_{21}H_{17}O_{11}$	445.07653	445.07849	13.5	1.922	269(100),445(28),113 (13),85(7),71(5)	+	+	+	–	–	–	–
C9 (B5-B9)	N	5.63	$C_{21}H_{17}O_{11}$	445.07653	445.07822	13.5	1.315	269(100),445(45),113 (20),85(15),71(1)	+	+	+	–	–	–	–
	P	5.63	$C_{21}H_{19}O_{11}$	447.09218	447.09122	12.5	−0.968	114(100),99(70),139 (42),159(38),447(1)	+	+	+	+	–	–	–
C10 (B22-B25)	P	4.87	$C_{16}H_{13}O_7$	317.06557	317.06604	10.5	1.453	299(100),271(26),102 (10),225(4),317(2)	–	–	–	–	–	–	+
C11 (B34)	N	6.96	$C_{22}H_{19}O_5N_4$	419.13499	419.13513	15.5	−0.963	419(100),221(28),243 (43),373(2),263(1)	+	+	+	+	–	–	–
C12 (B35-B39)	N	6.64	$C_{22}H_{25}N_4O_4$	409.18703	409.18967	12.5	3.767	409(100),253(40),225 (11),211(11),201(3)	–	–	–	–	+	–	–
C13 (B35-B39)	N	6.81	$C_{22}H_{25}N_4O_4$	409.18703	409.18945	12.5	3.229	409(100),211(42),253 (16),325(6),201(4)	–	–	–	–	+	–	–
C14 (B35-B39)	N	7.59	$C_{22}H_{25}N_4O_4$	409.18703	409.18915	12.5	2.496	253(100),409(85),211 (40),327(23),227(14)	–	–	–	–	+	–	–
C15 (B35-B39)	N	7.78	$C_{22}H_{25}N_4O_4$	409.18703	409.18924	12.5	2.716	409(100),253(95),96 (44),327(28),201(26)	–	–	–	–	+	–	–
C16 (B35-B39)	N	7.96	$C_{22}H_{25}N_4O_4$	409.18703	409.18881	12.5	1.665	409(100),211(95),327 (26),253(21),96(16)	–	–	–	–	+	–	–
C17 (B35-B39)	N	8.51	$C_{22}H_{25}N_4O_4$	409.18703	409.18915	12.5	2.496	409(100),211(73),253 (48),171(18),329(12)	–	–	–	–	+	–	–
C18 (A2)	N	6.86	$C_{21}H_{21}O_9$	417.11911	417.11948	11.5	0.898	417(100),255(53),241 (38),163(36),59(19)	+	+	+	+	–	+	–
C19 (A3)	N	5.32	$C_{15}H_{13}O_6S$	321.04273	321.04376	9.5	−0.225	321(100),121(55),241 (33),80(26),135(15)	+	–	–	–	–	–	–
C20 (A3)	N	6.81	$C_{15}H_{13}O_6S$	321.04273	321.04388	9.5	0.149	321(100),121(53),241 (48),80(19),135(15)	+	+	+	–	–	+	–
C21 (A3)	N	6.98	$C_{15}H_{13}O_6S$	321.04273	321.04379	9.5	−0.131	321(100),121(49),241 (34),80(23),135(14)	+	+	+	–	–	+	–
C22 (A3)	N	7.16	$C_{15}H_{13}O_6S$	321.04273	321.04391	9.5	0.243	321(100),121(48),241 (34),219(27),80(20)	+	+	+	–	–	+	–
C23 (A3)	N	7.34	$C_{15}H_{13}O_6S$	321.04273	321.04410	9.5	0.834	321(100),121(55),219 (40),241(40),80(23)	+	+	+	–	–	+	–
C24 (A3)	N	7.53	$C_{15}H_{13}O_6S$	321.04273	321.04407	9.5	0.741	321(100),121(46),241 (44),219(30),80(25)	+	–	–	–	–	+	–
C25 (A5-A12)	N	5.71	$C_{16}H_{15}O_5$	287.09140	287.09274	9.5	0.847	213(100),287(62),257 (27),106(10),59(5)	–	–	–	–	+	–	–
C26 (A14)	P	5.93	$C_{18}H_{19}O_6$	331.11761	331.11707	9.5	−1.645	211(57),121(48),133(20),86 (20),331(1)	–	–	–	–	+	–	–
C27 (A14)	P	6.91	$C_{18}H_{19}O_6$	331.11761	331.11768	9.5	0.197	95(100),81(93),121(71),107 (67),331(2)	–	–	–	–	+	–	–
C28 (A14)	N	7.70	$C_{18}H_{17}O_6$	329.10196	329.10303	10.5	−0.096	329(100),311(22),284 (15),269(14),239(1)	–	–	–	–	+	–	–
C29 (A14)	P	2.79	$C_{19}H_{20}NO_4S$	358.11075	358.11053	10.5	−0.629	84(100),129(94),179 (58),358(48),105(48)	–	–	–	–	+	–	–

(*continued on next page*)

Table 1c (*continued*)

ID	Ion Mode	t_R/ min	Formula $[M-H]^-$/ $[M+H]^+$	Theoretical Mass (*m/z*)	Experimental Mass (*m/z*)	RDB	Error (ppm)	MS/MS Fragment Ions	PS	PM	PA	U	F	L	LM
C30	N	9.98	$C_{26}H_{24}O_{10}N_3S$	570.11769	570.11871	16.5	−0.136	570(100),163(82),500 (34),534(20),126(9)	+	−	+	−	−	−	−
C31	N	11.01	$C_{26}H_{24}O_{10}N_3S$	570.11769	570.11920	16.5	0.723	534(100),570(32),163 (31),128(16),496(9)	+	−	−	−	−	−	−

accuracy of metabolite identification.

Most importantly, the recursive tree strategy is simple, accurate, and convenient, and can be widely applied to the study of drug metabolites. The primary branching metabolites identified based on this strategy are regarded as the material basis for the treatment of diseases due to their high blood concentrations and well-defined molecular structures. In the present study, the recursive tree strategy was combined with network pharmacology, which not only comprehensively identified the metabolites of formononetin, but also improved the study of the mechanism of action of formononetin against NAFLD. The innovative initiative is of great significance as it lays the foundation for the identification of drug metabolites and their pharmacological activity studies.

4.2. Comparison of formononetin metabolites in vivo and in vitro

Biotransformation is a featured segment of drug metabolism research. Most of the metabolism studies in the crowd are mainly based on rats. Of interest is the rapidity and simplicity of microsome metabolism assays *in vitro*. The selective interaction between enzymes and substrates can be directly observed, reducing the interference of many internal factors (Knights et al., 2016). Therefore, microsomes can serve as a reliable source for *in vivo* and *in vitro* overall research. Among them, liver microsomes are the most effective means because they contain a variety of hepatic drug enzymes (Chen et al., 2023). At present, there have been no reports on the *in vivo* and *in vitro* metabolism of formononetin. Thus, a recursive tree analysis strategy and LC-HRMS were used to compare the metabolism of formononetin in rats and liver microsomes with a view to retrieve the metabolites of formononetin more comprehensively.

In the *in vivo* study, 53, 27, 46, and 9 metabolites were detected in rat plasma, urine, faeces, and liver, respectively. Although there were fewer metabolites in the liver, it might be the result of rapid metabolism by multiple enzymes. In addition, plasma, urine, and faeces have higher metabolic activity, and most of the metabolites were excreted through urine and faeces. Genistein (**B9**) was detected in plasma and urine as one of the important metabolites of formononetin. It has various pharmacological properties, including tyrosine and topoisomerase inhibition (Cheng et al., 2023; Jaiswal et al., 2019). In addition, the demethylated metabolite Daidzein (**A2**) was detected in plasma, urine, and faeces. The pharmacological effects of Daidzein, a typical isoflavone, have been extensively studied, including anti-inflammatory, hypolipidemic, antitumor, and neuroprotective effects (Pyo et al., 2009; Zhu et al., 2021; Grisley et al., 2022). It was worth mentioning that only 9 metabolites, mostly tertiary branching metabolites, were detected in the liver, even though it was the most important metabolic organ in the body. As a consequence, preliminary speculation suggested that formononetin was rapidly metabolized by hepatic drug enzymes, prone to multi-level reactions, and excreted from the body by urine and faeces *via* internal circulation.

In vitro study, liver microsomes also exhibited strong metabolism, and although fewer formononetin metabolites were found in liver microsomes than in rats, most phase II metabolites were shown. More importantly, Ononin (**A1**) was found only in liver microsomes. It indicated that the metabolic conversion of ononin to other metabolites occurred rapidly in the body. Currently, there were more studies on ononin, which was widely used in clinical practice and has clear pharmacological effects such as anti-inflammatory (Yu et al., 2023), anti-cancer (Ye et al., 2022), and anti-angiogenic (Fedoreyev et al., 2008). Overall, the metabolism of formononetin was much more complex *in vivo* than *in vitro*, but metabolism *in vitro* enriches the lack of biotransformation *in vivo* and provides a comprehensive database for the study of formononetin metabolism.

4.3. Comparison of the different biological treatment methods

The aim of sample preparation is to eliminate the interference of impurities with an appropriate recovery rate. Plasma samples are the most commonly used samples in metabolic assays and usually provide a good response to the overall level of the organism. It contains inorganic salts, oxygen, hormones, enzymes, antibodies, and cellular metabolites (Frampton et al., 2023). Due to the large number of proteins in plasma, precipitation is required prior to mass spectrometry analysis. Currently, researchers often use methanol and acetonitrile as protein precipitation reagents. The mechanism is to use organic solvents to disrupt the protein structure in biological samples, which reduces the solubility of proteins in aqueous solutions and thus converts them into solids for separation. Moreover, SPE is a sample preparation technique developed from chromatographic columns for extraction, separation, and concentration, using the difference in the interaction of different substances in the solid–liquid phases to achieve separation (Jordan et al., 2009). Hence, the plasma samples were first adsorbed onto the stationary phase and then eluted step by step using solvents with different elution capacities to achieve separation, purification, and enrichment.

The number and type of metabolites obtained by the three preparation methods used for the plasma samples were different. 49, 39, and 34 metabolites were obtained by the SPE method, methanol precipitation method, and acetonitrile precipitation method, respectively. Obviously, the SPE method yielded the highest number of metabolites and might be the best method for metabolite acquisition. Surprisingly, a large number of identical metabolites were obtained in both methanol and acetonitrile treatments. This also suggests that methanol can be chosen for protein precipitation in metabolite studies as it is cheap and easily available. The results in Table 1 showed that the samples prepared by SPE were mostly secondary and tertiary branching metabolites, specifically demethylated, sulfated, and glucuronidated metabolites. In contrast, arginine conjugation metabolites were predominantly captured in methanol and acetonitrile precipitations. (See Table 1a-1d.).

The differences in the metabolites obtained by the three methods were due to a variety of reasons, including the influence of the matrix, the strength of the purification ability, and the divergence in separation options. A series of factors resulted in different intensity and quantity signal peaks of formononetin metabolites after UPLC-HRMS detection.

4.4. Potential metabolic pathways of formononetin

The elucidation of the drug metabolic pathways can help the in-depth study of the pharmacological mechanisms. In the present study, the metabolites of formononetin were identified for the first time based on the recursive tree analysis strategy. There were 20, 42, 32, and 37 metabolites with primary, secondary, tertiary and multistage branches, respectively. The analysis revealed that there was a universal phase I and phase II metabolic process for formononetin, and the metabolic

Table 1d
Multi-level branching metabolites of formononetin **(D1-D37)**.

ID	Ion Mode	t_R/ min	Formula $[M-H]^-$/ $[M+H]^+$	Theoretical Mass (*m/z*)	Experimental Mass (*m/z*)	RDB	Error (ppm)	MS/MS Fragment Ions	PS	PM	PA	U	F	L	LM
D1 (C3)	N	7.22	$C_{21}H_{21}O_{10}$	433.11292	433.11414	11.5	0.120	433(100),257(94),271(64),415(40),175(30)	–	+	+	–	+	–	–
D2 (C12-C17)	N	7.27	$C_{22}H_{25}N_4O_3$	393.19211	393.19339	12.5	0.448	79(100),393(77),191(9),81(2),171(2)	–	–	–	–	+	–	–
D3 (C12-C17)	N	7.63	$C_{22}H_{25}N_4O_3$	393.19211	393.19339	12.5	0.448	79(100),393(88),191(8),96(3),171(2)	–	–	–	–	+	–	–
D4 (C12-C17)	N	7.82	$C_{22}H_{25}N_4O_3$	393.19211	393.19391	12.5	1.770	393(100),79(89),59(8),96(5),165(4)	–	–	–	–	+	–	–
D5 (C12-C17)	N	8.69	$C_{22}H_{25}N_4O_3$	393.19211	393.19296	12.5	−0.646	393(100),80(77),311(21),116(4),191(3)	–	–	–	–	+	–	–
D6 (C12-C17)	N	9.24	$C_{22}H_{25}N_4O_3$	393.19211	393.19354	12.5	0.829	80(100),393(68),311(40),62(16),171(3)	–	–	–	–	+	–	–
D7 (C12-C17)	N	10.00	$C_{22}H_{25}N_4O_3$	393.19211	393.19205	12.5	−2.960	80(100),393(82),311(32),293(20),61(11)	–	–	–	–	+	–	–
D8 (C18)	N	7.05	$C_{20}H_{21}O_7$	373.12817	373.12967	10.5	0.394	329(100),373(84),284(58),147(30),175(25)	+	+	–	–	–	–	–
D9 (C18)	N	10.04	$C_{20}H_{21}O_7$	373.12817	373.13278	10.5	3.504	373(100),293(98),275(66),80(28),64(13)	+	+	–	–	–	–	–
D10 (C18)	P	10.97	$C_{20}H_{23}O_7$	375.14382	375.14459	9.5	2.027	375(100),189(34),213(11),199(11),357(5)	–	–	–	–	–	–	+
D11 (C18)	N	5.27	$C_{20}H_{19}O_8$	387.10744	387.10858	11.5	0.101	387(100),134(65),96(42),149(26),80(26),	–	–	–	–	+	–	–
D12 (C18)	N	5.45	$C_{20}H_{19}O_8$	387.10744	387.10794	11.5	−1.552	387(100),134(76),193(50),80(48),171(16)	–	–	–	–	+	–	–
D13 (C18)	N	5.83	$C_{20}H_{19}O_8$	387.10744	387.10822	11.5	−0.829	387(100),343(34),80(31),134(24),284(18)	–	–	–	–	+	–	–
D14 (C18)	N	7.60	$C_{20}H_{19}O_8$	387.10744	387.11099	11.5	2.449	113(100),387(71),196(56),85(54),59(30)	+	–	–	–	–	–	–
D15 (C18)	P	10.77	$C_{20}H_{21}O_8$	389.12309	389.12308	10.5	−0.036	389(100),189(36),174(28),136(21),81(10)	–	–	–	–	–	–	+
D16 (C18)	N	6.96	$C_{21}H_{23}O_9$	419.13365	419.13513	10.5	0.375	419(100),113(55),243(43),85(36),59(19)	+	+	+	+	–	–	–
D17 (C18)	P	6.22	$C_{21}H_{21}O_8$	401.12309	401.12076	11.5	−2.334	401(80),131(18),145(14),84(13),119(13)	+	–	+	+	–	–	–
D18 (C18)	N	5.23	$C_{21}H_{21}O_{12}S$	497.07482	497.07614	11.5	0.443	321(100),497(39),241(25),113(17),85(11)	+	+	+	+	–	–	–
D19 (C18)	N	5.41	$C_{21}H_{21}O_{12}S$	497.07482	497.07645	11.5	1.066	321(100),497(39),241(25),113(17),85(11)	+	+	+	–	–	–	–
D20 (C18)	N	5.58	$C_{21}H_{21}O_{12}S$	497.07482	497.07620	11.5	0.563	321(100),497(43),241(26),113(22),80(10)	+	+	+	–	–	–	–
D21 (C18)	N	5.76	$C_{21}H_{21}O_{12}S$	497.07482	497.07697	11.5	2.112	321(100),497(40),241(26),113(20),85(8)	+	–	–	–	–	–	–
D22 (D2-D7)	N	12.30	$C_{22}H_{27}N_4O_3$	395.20776	395.20993	11.5	2.697	395(100),96(94),315(27),268(7),59(5)	–	–	–	+	+	–	–
D23 (D18-D21)	N	5.66	$C_{21}H_{21}O_{13}S$	513.06973	513.07196	11.5	1.125	269(100),467(89),514(27),113(19),391(14)	+	+	+	–	–	–	–
D24 (D22)	N	7.31	$C_{22}H_{27}N_4O$	363.21793	363.21829	11.5	−2.051	363(100),317(19),57(11),80(10),261(4)	–	–	–	–	+	–	–
D25 (D22)	N	8.38	$C_{22}H_{27}N_4O$	363.21793	363.21814	11.5	−2.464	363(100),96(29),80(14),201(11),171(9)	–	–	–	–	+	–	–
D26 (D22)	N	8.75	$C_{22}H_{27}N_4O$	363.21793	363.21909	11.5	0.152	363(100),80(31),345(21),96(15),123(6)	–	–	–	–	+	–	–
D27 (D22)	N	9.27	$C_{22}H_{27}N_4O$	363.21793	363.21802	11.5	−2.794	363(100),317(17),171(4),201(3),80(1)	–	–	–	–	+	–	–
D28 (D22)	N	9.45	$C_{22}H_{27}N_4O$	363.21793	363.21841	11.5	−1.720	363(100),96(7),80(5),191(4),317(2)	–	–	–	–	+	–	–
D29 (B31)	P	5.79	$C_{16}H_{19}O$	227.14304	227.14249	7.5	−2.429	213(100),150(92),210(79),107(52),227(36)	–	–	–	–	+	–	–
D30 (B31)	P	7.65	$C_{16}H_{19}O$	227.14304	227.14310	7.5	0.256	81(91),227(85),95(68),184(61),107(61)	–	–	–	–	+	–	–
D31 (B31)	P	11.16	$C_{16}H_{19}O$	227.14304	227.14328	7.5	1.049	71(100),81(29),95(15),135(11),227(6)	–	–	–	–	+	–	–
D32 (B35-B39)	N	9.78	$C_{22}H_{23}N_4O_2$	375.18155	375.18433	13.5	−1.224	80(100),375(94),293(46),63(21),171(5)	–	–	–	–	+	–	–
D33 (B35-B39)	N	9.95	$C_{22}H_{23}N_4O_2$	375.18155	375.18433	13.5	1.681	80(100),375(89),64(47),116(25),191(21)	+	–	–	–	+	–	–
D34 (B35-B39)	N	10.17	$C_{22}H_{23}N_4O_2$	375.18155	375.18423	13.5	1.581	375(100),80(90),64(49),191(28),293(19)	+	–	–	–	+	–	–
D35	P	7.29	$C_{15}H_7O_2$	219.04405	219.04480	12.5	3.397	201(65),159(43),119(34),103(14),219(4)	–	–	–	–	+	–	–
D36	N	3.50	$C_{18}H_{16}NO_3S$	326.08454	326.08807	11.5	2.433	108(100),326(90),150(85),173(66),85(37)	–	+	+	–	–	–	–

(*continued on next page*)

Table 1d (*continued*)

ID	Ion Mode	t_R/ min	Formula $[M-H]^-$/ $[M+H]^+$	Theoretical Mass (*m/z*)	Experimental Mass (*m/z*)	RDB	Error (ppm)	MS/MS Fragment Ions	PS	PM	PA	U	F	L	LM
	P	3.55	$C_{18}H_{18}NO_3S$	328.10019	328.10138	10.5	3.625	152(100),110(85),85(8),120(4),328(4)	–	–	–	+	–	–	–
D37	N	2.36	$C_{18}H_{20}NO_4S$	346.11075	346.10828	9.5	−3.572	346(100),316(46),241(38),127(28),104(24)	–	+	–	–	–	–	–

Note: t_R: retention time; PS: SPE column treated plasma; PM: Methanol treated plasma; PA: Acetonitrile treated plasma; U: urine; F: faeces; L: liver; LM: liver microsomes; "+": detected; "-": undetected. The recursive branching metabolites were marked in the lower right corner of the ID.

pathways included demethylation, decarbonylation, methylation, hydroxylation, sulfation, glucuronidation, arginine conjugation, glutathione conjugation, and their complex reactions, *etc*. The metabolic profile of formononetin was shown in Fig. 3. Significantly, the most metabolites were identified in plasma, followed by faeces and urine, while the fewest metabolites were identified in the liver. We speculated that after oral administration, formononetin might be biotransformed with the participation of gastric acid, digestive enzymes, and intestinal flora. After absorption into the blood, it is rapidly metabolized by the kidneys and liver and then excreted in the faeces and urine.

Understanding the metabolic properties of drugs is of great significance for drug development and clinical treatment. Formononetin is a typical isoflavone component with low polarity. Therefore, it mostly exists in organisms as hydroxylation products and conjugation products such as sulfation and glucuronidation, increasing the polarity to facilitate absorption and excretion. For example, Ononin (**A1**), Daidzein (**A2**), Formononetin-7-O-sulfate (**A3**), Formononetin-7-O-GluA (**A4**), Calycosin (**A8** or **A9**), Biochanin A (**A12**), Dihydroformononetin (**A14**), Formononetin-7-O-Arg (**A15**), Genistein (**B9**), *etc*.

4.5. Formononetin attenuated PA/OA-induced lipid accumulation and oxidative stress

NAFLD is a disease caused by excessive fat deposition in the liver in addition to alcohol and other liver damage factors, and is recognized as the most common metabolic liver disease worldwide (Nian et al., 2023). NAFLD can progress from simple steatosis at the beginning to hepatitis and finally to cirrhosis and liver cancer, with a prevalence of about 25 % in adults (Jiang et al., 2023). Studies have proven that NAFLD has a long course and complex pathogenesis, which is still unclear. During the development of NAFLD, lipid metabolism disorders cause lipid accumulation. This process results in a high accumulation of ROS inducing oxidative stress in the liver. In turn, the mitochondrial dysfunction induced by oxidative stress may cause oxidative damage, which triggers a series of cascade signals leading to inflammation, cell death, and fibrosis (Loh et al., 2023). Therefore, inhibition of the inflammatory response and antioxidant may be effective in the treatment of NAFLD. At present, only some hepatoprotective and lipid-lowering drugs can be used clinically, and there is no specific drug on the market. The search for safe and effective anti-NAFLD drugs is imminent.

Our *in vitro* experiments preliminarily demonstrated that TG and TC levels were significantly elevated and lipid droplet aggregation was obvious in HepG2 cells induced by PA/OA. Formononetin treatment significantly reduced lipid accumulation. Oxidative stress is considered to be a key pathogenic link in the development of NAFLD (Fang et al., 2023). Dysregulation of SOD and GSH predisposes to mitochondrial dysfunction and the production of pro-inflammatory factors such as IL-6 and TNF-α (Meca et al., 2021). However, with the accumulation of lipids in the liver, the increased metabolism of free fatty acids and lipopolysaccharides leads to increased ROS production, accelerating oxidative stress and inflammatory responses in the liver (Gao et al., 2022). As stated, AST, ALT, and GSH levels were significantly elevated in PA/OA-induced HepG2 cells, whereas SOD levels were significantly decreased. However, the above indicators were reversed after treatment with formononetin. Our data suggest that formononetin ameliorated PA/OA-induced NAFLD.

4.6. Prediction of the mechanism of formononetin against NAFLD

To investigate the possible mechanisms of formononetin intervening in NAFLD, we evaluated the mechanism of action of formononetin and its primary branching metabolites against NAFLD using network pharmacology. As a result, it was indicated that AKT1, ALB, TNF, STAT3, and EGFR were more important core targets, which played pharmacological roles in NAFLD. Among them, AKT1 is involved in insulin resistance and FoxO signaling pathways, and its high level of expression contributed to the severity in patients with NAFLD (Abolfazli et al., 2022). Members of the tumor necrosis factor protein family are among the most typical triggers of hepatocyte death, and overexpression of TNF-α triggers pro-apoptotic signaling in hepatic adipocytes (Shirakami et al., 2023). Furthermore, STAT3 is a promising therapeutic target. Activation of phosphorylated STAT3 is one of the predisposing factors for the development of NAFLD to hepatocellular carcinoma (Krizanac et al., 2023). In addition, EGFR is a cell membrane protein that can be activated by its ligand, epidermal growth factor. It has been shown that epidermal growth factor receptor deletion in mice not only reduced the accumulation of macrophages in the liver, but also reduced the release of inflammatory factors (Li et al., 2023). The amelioration of NAFLD was verified by EGFR knockout mice (Shao et al., 2023). Thus, reducing the expression of EGFR may be an effective breakthrough point for the treatment of NAFLD.

To further explore the mechanism of action of formononetin and its metabolites against NAFLD and provide a scientific basis for related experimental studies, the researchers performed GO and KEGG pathway enrichment analysis. GO analysis enriched these targets in the categories such as "response to hormone", "positive regulation of phosphorylation", "protein kinase activity", and "lytic vacuole". KEGG analysis pooled targets across multiple pathways, and signaling pathways with high gene counts included: pathways in cancer, lipid and atherosclerosis, MAPK signaling pathway, PI3K-Akt signaling pathway, and prostate cancer, *etc*. Among these, regulation of the PI3K-AKT pathway ameliorates hepatic oxidative stress and further inhibits NF-κB mediated inflammatory responses in NAFLD. Fang et al. (2023) found that the MAPK signaling pathway has a regulatory role in oxidative stress, mitochondrial dysfunction, and hepatic steatosis. Inhibiting the activation of the MAPK signaling pathway, abnormal metabolism, and oxidative stress could be alleviated to improve NAFLD. Lipid autophagy was considered a novel mechanism to regulate cellular lipid metabolism and lipid deposition (Liu et al., 2023). Activation of the AMPK/mTOR signaling pathway enhanced hepatic macrophage autophagy, which could further inhibit IL-17 mediated inflammatory response and thus significantly improved NAFLD-related liver injury (Meng et al., 2021). In addition, TNF-α has been found to play an important role in lipid accumulation. It first promotes lipid synthesis in the liver and activates adipokines leading to obesity. At the same time, it regulates the activity of lipid metabolizing enzymes and inhibits the uptake of free fatty acids leading to lipid accumulation in the liver (Peng et al., 2023). Therefore, the TNF signaling pathway has been concluded to be a predisposing pathway in the development of NAFLD and contributes to the advancement of NAFLD to NASH.

The results of the study revealed the potential mechanism of formononetin against NAFLD from the perspective of preliminary *in vitro* experiments and network pharmacology, but bioinformatics has limitations. We will next validate the network pharmacology results through pharmacological experiments and molecular biology techniques.

5. Conclusion

In the present study, an analytical strategy of recursive tree bridging network pharmacology provides a powerful integrated approach to identify drug metabolites and predict the pharmacological activity of metabolites. The validity of the strategy was validated for the first time by analyzing formononetin. As a result, a total of 131 metabolites were identified. Metabolic pathways included oxidation, methylation, hydrogenation, glucuronidation, sulfation, and their complex reactions. The primary branching metabolites collectively covered the candidate targets and enrichment pathways of formononetin against NAFLD. Thus, the bioactivity of formononetin against NAFLD might be mediated by formononetin itself and/or its multiple metabolites. Additionally, the anti-NAFLD effects of formononetin was verified by *in vitro* cellular assays. In brief, we have not only established a new strategy for metabolite analysis, but also enriched the database of metabolic transformations of formononetin. Its combination with network pharmacology provided effective information for subsequent pharmacological studies in NAFLD.

CRediT authorship contribution statement

Yanan Li: Data curation, Writing – original draft, Writing – review & editing, Investigation, Formal analysis. **Shaoping Wang:** Visualization. **Hong Wang:** Resources. **Long Dai:** Methodology, Supervision. **Jiayu Zhang:** Conceptualization, Funding acquisition.

Declaration of Competing Interest

The authors declare that they have no known competing financial interests or personal relationships that could have appeared to influence the work reported in this paper.

Acknowledgements

This work was supported by the National Natural Science Foundation of China, China (82174039), Natural Science Foundation of Shandong Province, China (ZR2020MH371), Taishan Young Scholar Program of Shandong, China (TSQN202103110), Chinese Medicine Science and Technology Program of Shandong Province, China (Z-2022085), and Matching Support Program for Provincial and Above Leading Talents in Yantai City, China (10073801).

Appendix A. Supplementary data

Supplementary data to this article can be found online at https://doi.org/10.1016/j.arabjc.2024.105761.

References

Abolfazli, P., Aghajanzadeh, T., Ghaderinasrabad, M., Apue Nchama, C.N., Mokhlesi, A., Talkhabi, M., 2022. Bioinformatics analysis reveals molecular connections between non-alcoholic fatty liver disease (NAFLD) and COVID-19. J Cell Commun Signal. 16 (4), 609–619.

Almazroo, O.A., Miah, M.K., Venkataramanan, R., 2017. Drug Metabolism in the Liver. Clin Liver Dis. 21 (1), 1–20.

Aly, S.H., Elissawy, A.M., Fayez, A.M., Eldahshan, O.A., Elshanawany, M.A., Singab, A.N. B., 2021. Neuroprotective effects of Sophora secundiflora, Sophora tomentosa leaves and formononetin on scopolamine-induced dementia. Nat Prod Res. 35 (24), 5848–5852.

Cai, W., Li, K.L., Xiong, P., Gong, K.Y., Zhu, L., Yang, J.B., Wu, W.H., 2020. A systematic strategy for rapid identification of chlorogenic acids derivatives in Duhaldea nervosa using UHPLC-Q-Exactive Orbitrap mass spectrometry. Arabian Journal of Chemistry. 13 (2), 3751–3761.

Chen, F., Zou, H., Zhang, P., Yan, Y., 2023. Investigation on the *in vitro* metabolism of bicyclol using liver microsomes, hepatocytes and human recombinant cytochrome P450 enzymes. Xenobiotica. 1–31. Advance online publication.

Cheng, Y., Tang, Y., Tan, Y., Li, J., Zhang, X., 2023. KCNK9 mediates the inhibitory effects of genistein on hepatic metastasis from colon cancer. Clinics (sao Paulo). 78, 100141.

Cui, Y.F., Zhang, W.W., Li, Y.N., Xu, J., Lan, X.M., Song, S.Y., Lin, Y.Q., Dai, L., Zhang, J. Y., 2022. The Analytical Strategy of "Ion Induction and Deduction Based on Net-Hubs" for the Comprehensive Characterization of Naringenin Metabolites *In Vivo* and *In Vitro* Using a UHPLC-Q-Exactive Orbitrap Mass Spectrometer. Molecules. 27 (21), 7282.

Das, D., Sarkar, S., Bordoloi, J., Wann, S.B., Kalita, J., Manna, P., 2018. Daidzein, its effects on impaired glucose and lipid metabolism and vascular inflammation associated with type 2 diabetes. Biofactors. 44 (5), 407–417.

Dong, F., Wang, S., Yang, A., Li, H., Dong, P., Wang, B., Dai, L., Lin, Y., Zhang, J., 2021. Characterization of Metabolites of α-mangostin in Bio-samples from SD Rats by UHPLC-Q-exactive Orbitrap MS. Curr Drug Metab. 22 (13), 1065–1073.

Fedoreyev, S.A., Bulgakov, V.P., Grishchenko, O.V., Veselova, M.V., Krivoschekova, O.E., Kulesh, N.I., Denisenko, V.A., Tchernoded, G.K., Zhuravlev, Y.N., 2008. Isoflavonoid composition of a callus culture of the relict tree Maackia amurensis Rupr. et Maxim. J Agric Food Chem. 56 (16), 7023–7031.

Frampton, J., Serrano-Contreras, J.I., Garcia-Perez, I., Franco-Becker, G., Penhaligan, J., Tan, A.S.Y., de Oliveira, A.C.C., Milner, A.J., Murphy, K.G., Frost, G., Chambers, E.S., 2023. The metabolic interplay between dietary carbohydrate and exercise and its role in acute appetite regulation in males: a randomized controlled study. J Physiol. https://doi.org/10.1113/JP284294. Advance online publication.

Gao, W., Xu, B., Zhang, Y., Liu, S., Duan, Z., Chen, Y., Zhang, X., 2022. Baicalin Attenuates Oxidative Stress in a Tissue-Engineered Liver Model of NAFLD by Scavenging Reactive Oxygen Species. Nutrients. 14 (3), 541.

Grisley, E.D., Huber, K.N., Knapp, A.N., Butteiger, D.N., Banz, W.J., MacLean, J.A., Wallace, D.G., Cheatwood, J.L., 2022. Effects of Dietary Soy Protein Isolate Versus Isoflavones Alone on Poststroke Skilled Ladder Rung Walking and Cortical mRNA Expression Differ in Adult Male Rats. J Med Food. 25 (2), 158–165.

Guo, P., Dong, L., Yan, W., Wei, J., Wang, C., Zhang, Z., 2015. Simultaneous determination of linarin, naringenin and formononetin in rat plasma by LC-MS/MS and its application to a pharmacokinetic study after oral administration of Bushen Guchi Pill. Biomed Chromatogr. 29 (2), 246–253.

Jaiswal, N., Akhtar, J., Singh, S.P., Badruddeen, A., F., 2019. An Overview on Genistein and its Various Formulations. Drug Res. 69 (6), 305–313.

Jiang, W., Mao, X., Liu, Z., Zhang, T., Jin, L., Chen, X., 2023. Global Burden of Nonalcoholic Fatty Liver Disease, 1990 to 2019: Findings From the Global Burden of Disease Study 2019. J Clin Gastroenterol. 57 (6), 631–639.

Jing, X., Pingping, D., Yifang, C., Huajian, L., Shan, J., Yong, W., Jiayu, Z., 2022. Comprehensive analysis of dihydromyricetin metabolites in rats using ultra-high-performance liquid chromatography coupled with high-resolution mass spectrometry. J Sep Sci. 45 (21), 3930–3941.

Jordan, T.B., Nichols, D.S., Kerr, N.I., 2009. Selection of SPE cartridge for automated solid-phase extraction of pesticides from water followed by liquid chromatography-tandem mass spectrometry. Anal Bioanal Chem. 394 (8), 2257–2266.

Kaur, G., Gupta, S.K., Singh, P., Ali, V., Kumar, V., Verma, M., 2020. Drug-metabolizing enzymes: role in drug resistance in cancer. Clin Transl Oncol. 22 (10), 1667–1680.

Kim, J.H., Kang, D.W., Cho, S.J., Cho, H.Y., 2022. Parent-Metabolite Pharmacokinetic Modeling of Formononetin and Its Active Metabolites in Rats after Oral Administration of Formononetin Formulations. Pharmaceutics. 15 (1), 45.

Knights, K. M., Stresser, D. M., Miners, J. O., Crespi, C. L., 2016. *In Vitro* Drug Metabolism Using Liver Microsomes. Curr Protoc Pharmacol. 74, 7.8.1–7.8.24.

Krizanac, M., Mass Sanchez, P.B., Schröder, S.K., Weiskirchen, R., Asimakopoulos, A., 2023. Lipid-Independent Regulation of PLIN5 via IL-6 through the JAK/STAT3 Axis in Hep3B Cells. Int J Mol Scis. 24 (8), 7219.

Li, J., Li, C., Gou, J., Wang, X., Fan, R., Zhang, Y., 2016. An Alternative Pathway for Formononetin Biosynthesis in Pueraria lobata. Front Plant Sci. 7, 861.

Li, H.F., Li, T., Yang, P., Wang, Y., Tang, X.J., Liu, L.J., Xu, F., Shang, M.Y., Liu, G.X., Li, Y.L., Wang, X., Yin, J., Cai, S.Q., 2020. Global Profiling and Structural Characterization of Metabolites of Ononin Using HPLC-ESI-IT-TOF-MSn After Oral Administration to Rats. J Agric Food Chem. 68 (51), 15164–15175.

Li, L., Xiong, Y., Cao, W., Chen, Z., He, L., Tong, M., Zhang, L., Wu, M., 2023. Epidermal growth factor receptor promotes high-fructose nonalcoholic fatty liver disease by inducing mitochondrial fission in zebrafish. Biochem Biophys Res Commun. 652, 112–120.

Liu, X., Li, X., Su, S., Yuan, Y., Liu, W., Zhu, M., Zheng, Q., Zeng, X., Fu, F., Lu, Y., Chen, Y., 2023. Oleic acid improves hepatic lipotoxicity injury by alleviating autophagy dysfunction. Exp Cell Res. 429 (2), 113655. Advance online publication.

Liu, F., Pei, S., Li, W., Wang, X., Liang, C., Yang, R., Zhang, Z., Yao, X., Fang, D., Xie, S., Sun, H., 2021. Characterization of Formononetin Sulfonation in SULT1A3 Overexpressing HKE293 Cells: Involvement of Multidrug Resistance-Associated Protein 4 in Excretion of Sulfate. Front Pharmacol. 11, 614756.

Loh, C.H., Kuo, W.W., Lin, S.Z., Shih, C.Y., Lin, P.Y., Situmorang, J.H., Huang, C.Y., 2023. PKC-δ-dependent mitochondrial ROS attenuation is involved as 9-OAHSA combats lipoapotosis in rat hepatocytes induced by palmitic acid and in Syrian hamsters induced by high-fat high-cholesterol high-fructose diet. Toxicol Appl Pharmacol. 470, 116557.

Meca, A.D., Turcu-Stiolica, A., Stanciulescu, E.C., Andrei, A.M., Nitu, F.M., Banita, I.M., Matei, M., Pisoschi, C.G., 2021. Variations of Serum Oxidative Stress Biomarkers under First-Line Antituberculosis Treatment: A Pilot Study. J Pers Med. 11 (2), 112.

Meng, Z., Liu, X., Li, T., Fang, T., Cheng, Y., Han, L., Sun, B., Chen, L., 2021. The SGLT2 inhibitor empagliflozin negatively regulates IL-17/IL-23 axis-mediated inflammatory

responses in T2DM with NAFLD via the AMPK/mTOR/autophagy pathway. Int Immunopharmacol. 94, 107492.
Muñoz, M.T., Maldonado, V., Herrera, W., Mutis, A., Bardehle, L., Medina, C., Hormazábal, E., Ortega, F., Quiroz, A., 2022. Optimization of enzymatic parameters for the production of formononetin from red clover (Trifolium pratense L.) through a response surface methodology. Nat Prod Res. 36 (18), 4719–4724.
Nian, F., Zhu, C., Jin, N., Xia, Q., Wu, L., Lu, X., 2023. Gut microbiota metabolite TMAO promoted lipid deposition and fibrosis process via KRT17 in fatty liver cells in vitro. Biochem Biophys Res Commun. 669, 134–142.
Peng, C., Li, J., Ke, X., Liu, F., Huang, K.E., 2023. In silico and in vivo demonstration of the regulatory mechanism of Qi-Ge decoction in treating NAFLD. Ann Med. 55 (1), 2200258.
Rao, T., Gong, Y.F., Peng, J.B., Wang, Y.C., He, K., Zhou, H.H., Tan, Z.R., Lv, L.Z., 2019. Comparative pharmacokinetic study on three formulations of Astragali Radix by an LC-MS/MS method for determination of formononetin in human plasma. Biomed Chromatogr. 33 (9), e4563.
Shao, F., Deng, H., Zhang, W., Ren, Z., Kang, Z., Ding, Z., Zhang, J., Zang, Y., 2023. Loss of EGFR contributes to high-fat diet-induced nonalcoholic fatty liver disease. FEBS Lett. 597 (11), 1503–1516.
Shirakami, Y., Kato, J., Maeda, T., Ideta, T., Imai, K., Sakai, H., Shiraki, M., Shimizu, M., 2023. Skeletal muscle atrophy is exacerbated by steatotic and fibrotic liver-derived TNF-α in senescence-accelerated mice. J Gastroenterol Hepatol. 38 (5), 800–808.
Wang, H., Xu, J., Dong, P., Li, Y., Cui, Y., Li, H., Li, H., Zhang, J., Wang, S., Dai, L., 2022. Comprehensive Analysis of Pterostilbene Metabolites *In Vivo* and *In Vitro* Using a UHPLC-Q-Exactive Plus Mass Spectrometer with Multiple Data-Mining Methods. ACS Omega. 7 (43), 38561–38575.
Wang, Y., Zhao, H., Li, X., Wang, Q., Yan, M., Zhang, H., Zhao, T., Zhang, N., Zhang, P., Peng, L., Li, P., 2019. Formononetin alleviates hepatic steatosis by facilitating TFEB-mediated lysosome biogenesis and lipophagy. J Nutr Biochem. 73, 108214.
Ye, B., Ma, J., Li, Z., Li, Y., Han, X., 2022. Ononin Shows Anticancer Activity Against Laryngeal Cancer via the Inhibition of ERK/JNK/p38 Signaling Pathway. Front Oncol. 12, 939646.
Yin, J., Zhang, X., Zhang, Y., Ma, Y., Li, L., Li, D., Zhang, L., Zhang, Z., 2019. Comprehensive Study of the *in Vivo* and *in Vitro* Metabolism of Dietary Isoflavone Biochanin A Based on UHPLC-Q-TOF-MS/MS. J Agric Food Chem. 67 (45), 12481–12495.
Yu, T., Lu, X., Liang, Y., Yang, L., Yin, Y., Chen, H., 2023. Ononin alleviates DSS-induced colitis through inhibiting NLRP3 inflammasome via triggering mitophagy. Immun Inflamm Dis. 11 (2), e776.
Yu, L., Zhang, Y., Chen, Q., He, Y., Zhou, H., Wan, H., Yang, J., 2022. Formononetin protects against inflammation associated with cerebral ischemia-reperfusion injury in rats by targeting the JAK2/STAT3 signaling pathway. Biomed Pharmacother. 149, 112836.
Zhao, L., Han, J., Liu, J., Fan, K., Yuan, T., Han, J., Chen, L., Zhang, S., Zhao, M., Duan, J., 2021. A Novel Formononetin Derivative Promotes Anti-ischemic Effects on Acute Ischemic Injury in Mice. Front Microbiol. 12, 786464.
Zhu, Y., Yang, Z., Xie, Y., Yang, M., Zhang, Y., Deng, Z., Cai, L., 2021. Investigation of inhibition effect of daidzein on osteosarcoma cells based on experimental validation and systematic pharmacology analysis. PeerJ. 9, e12072.